Eur. Phys. J. C (2018) 78:109
https://doi.org/10.1140/epjc/s10052-018-5584-8

THE EUROPEAN PHYSICAL JOURNAL C

Regular Article - Theoretical Physics

"Spin-dependent" $\mu \to e$ conversion on light nuclei

Sacha Davidson[1,2,3,a], **Yoshitaka Kuno**[4], **Albert Saporta**[1,2,3]

[1] IPNL, CNRS/IN2P3, 4 Rue E. Fermi, 69622 Villeurbanne Cedex, France
[2] Université Claude Bernard Lyon 1, Villeurbanne, France
[3] Université de Lyon, 69622 Lyon, France
[4] Department of Physics, Osaka University, 1-1 Machikaneyama, Toyonaka, Osaka 560-0043, Japan

Received: 25 October 2017 / Accepted: 23 January 2018 / Published online: 6 February 2018

Abstract The experimental sensitivity to $\mu \to e$ conversion will improve by four or more orders of magnitude in coming years, making it interesting to consider the "spin-dependent" (SD) contribution to the rate. This process does not benefit from the atomic-number-squared enhancement of the spin-independent (SI) contribution, but probes different operators. We give details of our recent estimate of the spin-dependent rate, expressed as a function of operator coefficients at the experimental scale. Then we explore the prospects for distinguishing coefficients or models by using different targets, both in an EFT perspective, where a geometric representation of different targets as vectors in coefficient space is introduced, and also in three leptoquark models. It is found that comparing the rate on isotopes with and without spin could allow one to detect spin-dependent coefficients that are at least a factor of few larger than the spin-independent ones. Distinguishing among the axial, tensor and pseudoscalar operators that induce the SD rate would require calculating the nuclear matrix elements for the second two. Comparing the SD rate on nuclei with an odd proton vs. odd neutron could allow one to distinguish operators involving u quarks from those involving d quarks; this is interesting because the distinction is difficult to make for SI operators.

1 Introduction

Charged lepton flavour violation (CLFV) is new physics that must exist; only the rates are unknown. In this paper, we consider $\mu \leftrightarrow e$ flavour change, and assume that it can be parametrised by contact interactions involving Standard Model particles. Flavour change $\mu \leftrightarrow e$ can be probed in the decays $\mu \to e\gamma$ [1] and $\mu \to e\bar{e}e$ [2], in $\mu \to e$ conversion [3–5] and in various meson decays such as $K \to \bar{\mu}e$ [6]. In $\mu \to e$ conversion, a beam of μ^- impinges on a target, where the μ is captured by a nucleus, and can convert to an electron while in orbit. The COMET [7] and Mu2e [8] experiments, currently under construction, plan to improve the sensitivity by four orders of magnitude, reaching a branching ratio $\sim 10^{-16}$. The PRISM/PRIME proposal [9] aims to probe $\sim 10^{-18}$. These exceptional improvements in experimental sensitivity motivate our interest in subdominant contributions to $\mu \to e$ conversion.

Initial analytic estimates of the $\mu \to e$ conversion rate were performed by Feinberg and Weinberg [10], for promising operators and nuclei. A wider range of nuclei were studied numerically by Shanker [11], and estimates for many operators and nuclei can be found in the review [12]. Relativistic effects relevant in heavier nuclei were included in [13]. The matching of CLFV operators constructed with quarks and gluons, onto operators constructed with nucleons, was performed in [15]. The current state of the art is the detailed numerical calculations of Kitano, Koike and Okada (KKO) [14], who studied all the CLFV nucleon operators that contribute *coherently* to $\mu \to e$ conversion, for nuclei from helium to uranium. In such processes, the amplitude for $\mu \to e$ conversion on each nucleon is coherently summed over the whole nucleus. Like "spin-independent" (SI) dark matter scattering, the final rate therefore is enhanced by a factor $\sim A^2$, where A is the atomic number of the nucleus. However, other conversion processes are possible. For instance, incoherent $\mu \to e$ conversion, where the final-state nucleus is in an excited state, has been discussed by various people [11,16,17], and is expected to be subdominant with respect to the coherent process.

In a previous letter [18], some of us noted that "spin-dependent" (SD) $\mu \to e$ conversion can also occur, if the target nuclei have spin (as is the case for aluminium, the target of the upcoming COMET and Mu2e experiments). Although this process does not benefit from the $\sim A^2$ enhancement

[a] e-mail: s.davidson@ipnl.in2p3.fr

associated to SI rates, it has the interest of being mediated by different CLFV operators from the coherent process.

The aim of this manuscript is to give details of our calculation, and explore whether the SD process could help distinguish models or operators, should $\mu \to e$ conversion be observed. The operators which could induce SD $\mu \to e$ conversion are listed in Sect. 2. The conversion rate in aluminium is estimated in Sect. 3, and the extrapolation to other nuclei is discussed in Sect. 3.2. The theoretical uncertainties in our estimates are briefly discussed in Sect. 4. Section 5 explores the consequences of including the SD contribution to the $\mu \to e$ conversion rate, both in the perspective of obtaining constraints on operator coefficients from an upper bound on the branching ratio, and for discriminating models when $\mu \to e$ conversion is observed. This section comes in three parts: we study three leptoquark models which induce SD and SI conversion, then consider the same operators but with arbitrary coefficients, and calculate a covariance matrix. Finally, we allow all possible operators with arbitrary coefficients. We summarise in Sect. 6.

In our previous letter [18], we showed that the SI and SD operator coefficients mix under renormalisation group (RG) evolution between the experimental and weak scales. The effects of this mixing are significant: the largest contribution to the $\mu \to e$ conversion rate from an "SD" coefficient at the weak scale, would be via the RG mixing to an SI coefficient (for example, a tensor coefficient at the weak scale induces a SI contribution to the rate which is $\sim A^2$ larger than the SD contribution). In this paper, we focus on operator coefficients at the experimental scale, only including the RG evolution in the leptoquark models of Sect. 5.1. The RG evolution of the operator coefficients is summarised in Appendix C.

2 Operators

We are interested in contact interactions that can mediate $\mu \to e$ conversion on nuclei, at a scale $\mu_N \sim 2$ GeV. The focus of this manuscript is the subset of "spin-dependent" interactions, but for completeness, all QED $\times$ QCD invariant operators that mediate $\mu \to e$ conversion on nuclei are included. The relevant operators in the quark-level Lagrangian are [14,15]

$$\delta\mathcal{L} = -2\sqrt{2}G_F \sum_{Y\in L,R}\left[C_{D,Y}\mathcal{O}_{D,Y} + \frac{1}{m_t}C_{GG,Y}\mathcal{O}_{GG,Y} + \sum_{q=u,d,s}\sum_{O'} C^{qq}_{O',Y}\mathcal{O}^{qq}_{O',Y}\right] + h.c. \quad (1)$$

where the two-lepton operators are

$$\mathcal{O}_{D,Y} = m_\mu(\bar{e}\sigma^{\alpha\beta}P_Y\mu)F_{\alpha\beta}$$
$$\mathcal{O}_{GG,Y} = (\bar{e}P_Y\mu)G_{\alpha\beta}G^{\alpha\beta} \quad (2)$$

and $O' \in \{V, A, S, P, T\}$ labels two-lepton two-quark operators in a basis where only the lepton currents are chiral:

$$\mathcal{O}^{qq}_{V,Y} = (\bar{e}\gamma^\alpha P_Y\mu)(\bar{q}\gamma_\alpha q) \quad \mathcal{O}^{qq}_{A,Y} = (\bar{e}\gamma^\alpha P_Y\mu)(\bar{q}\gamma_\alpha\gamma_5 q)$$
$$\mathcal{O}^{qq}_{S,Y} = (\bar{e}P_Y\mu)(\bar{q}q), \quad \mathcal{O}^{qq}_{P,Y} = (\bar{e}P_Y\mu)(\bar{q}\gamma_5 q)$$
$$\mathcal{O}^{qq}_{T,Y} = (\bar{e}\sigma^{\alpha\beta}P_Y\mu)(\bar{q}\sigma_{\alpha\beta}q) \quad (3)$$

with $\sigma^{\alpha\beta} = \frac{i}{2}[\gamma^\alpha, \gamma^\beta]$ and $P_L = (1-\gamma_5)/2$. This choice of non-chiral quark currents is convenient for matching onto nucleons. However, often an operator basis with chiral quark currents is added to the Lagrangian as $\delta\mathcal{L} = -2\sqrt{2}G_F\sum C_{O,YX}\mathcal{O}^{qq}_{O,YX}$ [12,19,20], where, for instance, $\mathcal{O}^{qq}_{V,YX} \equiv (\bar{e}\gamma^\alpha P_Y\mu)(\bar{q}\gamma_\alpha P_X q)$. In this case, the coefficients are related by (recall that $\mathcal{O}^{qq}_{T,LR}$ vanishes—see Appendix C of [19])

$$C^{qq}_{V,Y} = \frac{1}{2}(C^{qq}_{V,YR} + C^{qq}_{V,YL}), \quad C^{qq}_{A,Y} = \frac{1}{2}(C^{qq}_{V,YR} - C^{qq}_{V,YL}),$$
$$C^{qq}_{S,Y} = \frac{1}{2}(C^{qq}_{S,YR} + C^{qq}_{S,YL}) \quad C^{qq}_{P,Y} = \frac{1}{2}(C^{qq}_{S,YR} - C^{qq}_{S,YL}),$$
$$C^{qq}_{T,Y} = C^{qq}_{T,YY}. \quad (4)$$

In Eq. (1), the coefficients and operators are evaluated close to the experimental scale, at $\mu_N \simeq 2$ GeV. The scale is relevant, because renormalisation group running mixes the tensor and axial vector operators (which induce SD $\mu \to e$ conversion) into the scalar and vector operators (who mediate the SI process) [18].[1] This is reviewed in Appendix C. Throughout the paper, coefficients without an explicit scale are assumed to be at μ_N.

To compute the rate for $\mu \to e$ conversion, the operators containing quarks should be matched at the scale μ_N onto CLFV operators involving nucleons and mesons. The relevant nucleon operators are the four-fermion operators of Eq. (3) with $q \to N$ and $N \in \{n, p\}$. As discussed below, rather than include mesons in the Lagrangian, we approximate their effects by form factors for some nucleon operators and two additional operators given in Eq. (10). So the nucleon-level Lagrangian will be

$$\delta\mathcal{L} = -2\sqrt{2}G_F \sum_{Y\in L,R}\left[C_{D,Y}\mathcal{O}_{D,Y} + \sum_{N=p,n}\sum_{O''}\widetilde{C}^{NN}_{O'',Y}\mathcal{O}^{NN}_{O'',Y}\right] + h.c. \quad (5)$$

where $O'' \in \{V, A, S, P, T, Der\}$.

At zero momentum transfer ($\vec{P}_f - \vec{P}_i \to 0$), we match onto operators with nucleon currents, by replacing

$$\bar{q}(x)\Gamma_O q(x) \to G^{N,q}_O \bar{N}(x)\Gamma_O N(x) \quad (6)$$

[1] The analogous mixing of SD WIMP scattering operators into SI operators was discussed in [21,22].

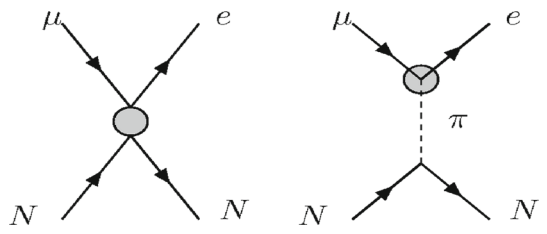

Fig. 1 Diagrams contributing to $\mu \to e$ conversion in the presence of axial and pseudoscalar CLFV operators (represented by the grey blob)

such that $\langle N|\bar{q}(x)\Gamma_O q(x)|N\rangle = G_O^{N,q}\langle N|\bar{N}(x)\Gamma_O N(x)|N\rangle = G_O^{N,q}\overline{u_N}(P_f)\Gamma_O u_N(P_i)e^{-i(P_f-P_i)x}$, with $\Gamma_O \in \{I, \gamma_5, \gamma^\alpha, \gamma^\beta\gamma_5, \sigma^{\alpha\beta}\}$. The constants $G_O^{N,q}$ obtained at zero-recoil are given in Appendix A, and we will assume that they are an acceptable approximation at the momentum-transfer of $\mu \to e$ conversion, which is $|\vec{P}_f - \vec{P}_i|^2 = m_\mu^2$.

Various mesons are present in the low energy theory at μ_N, so in principle the quark operators of Eq. (1) should be also matched onto meson operators. χPT [30] involving nucleons (see e.g. the review [23]) would be the appropriate formalism for this calculation, and it has been used to calculate WIMP scattering on nuclei [24–27], neutrinoless double beta decay [28], and SI $\mu \to e$ conversion [29]. However, to avoid more notation, here we just give results for the simple diagrams of interest. We only consider the CLFV decays of pions, because the effects of heavier mesons would be suppressed by their masses, and diagrams where a pion is exchanged between two nucleons are suppressed by more propagators, and would require two nucleons in the initial and final states.[2] Pion decay can contribute to $\mu \to e$ conversion via the second diagram of Fig. 1, in the presence of a pseudoscalar or axial vector quark current. We follow the notation of [23,30] in matching the axial vector and pseudoscalar quark currents onto the pion, at $P^2 = m_\pi^2$, as

$$\begin{aligned}\bar{q}(x)\tau^b\gamma^\alpha\gamma_5 q(x) &\to f_\pi i\partial^\alpha\pi^b(x),\\ 2m_q\bar{q}(x)\tau^3\gamma_5 q(x) &\to f_\pi m_\pi^2\pi^0(x)\end{aligned} \tag{7}$$

in order to obtain the usual expectation values $\langle 0|\bar{u}(x)\gamma^\alpha\gamma_5 d(x)|\pi^-(P)\rangle = \sqrt{2}P^\alpha f_\pi e^{-iP\cdot x}$, $\langle 0|\bar{u}(x)\gamma^\alpha\gamma_5 u(x)|\pi^0(P)\rangle = P^\alpha f_\pi e^{-iP\cdot x}$, and $\langle 0|\bar{u}(x)\gamma_5 u(x)|\pi(P)\rangle = f_\pi m_\pi^2 e^{-i\cdot Px}/2m_u$, where $f_\pi \simeq 92.4$ MeV.

Later in the manuscript, the matrix element for $\mu \to e$ conversion on a nucleon, $\mathcal{M}(\mu + N(P_i) \to e(k) + N(P_f))$ will be required. In the case of vector, scalar or tensor interactions, it is straightforward because conversion proceeds via a two-nucleon–two-lepton contact interaction. In the case of axial vector and pseudoscalar interactions, there is a pion exchange contribution, as illustrated in Fig. 1, so we give the matrix elements here. The pion–nucleon interaction term in the Lagrangian is taken as $ig_{\pi NN}\overline{N}\gamma_5\vec{\tau}\cdot\vec{\pi}N$, and the Goldberger–Treiman relation gives $g_{\pi pp} \simeq (G_A^{pu} - G_A^{pd})m_p/f_\pi$.

In the following two equations, $u_N = (u_p, u_n)$ represents a vector of spinors in isospin space. The matrix element $\mathcal{M}(\mu + N(P_i) \to e_X(k) + N(P_f))$ mediated by the axial up quark current, can be written [24,31]

$$\left(\overline{u_N}(P_f)\frac{[a_0 I + a_1\tau_3]}{2}\gamma^\alpha\gamma_5 u_N(P_i) + C_{A,X}^{uu}\frac{g_{\pi NN}f_\pi q^\alpha}{|q^2| + m_\pi^2}\overline{u_N}(P_f)[\tau_3]\gamma_5 u_N(P_i)\right)\overline{u_e}\gamma_\alpha P_X u_\mu \tag{8}$$

where $q = (0, -\vec{q}) = P_f - P_i$, the first term is written in terms of iso-scalar and iso-vector contributions $(a_0+a_1)/2 = C_{A,X}^{uu}G_A^{p,u}$, $(a_0 - a_1)/2 = C_{A,X}^{uu}G_A^{n,u}$, whereas the pion contribution is only isovector.

In the case of the pseudoscalar operator $\mathcal{O}_{P,Y}^{uu}$, the pion exchange diagram is non-vanishing at $|\vec{q}|^2 = 0$, so at finite momentum transfer, only the additional contribution $\propto 1/(|\vec{q}|^2 + m_\pi^2) - 1/m_\pi^2$ should be included. This gives

$$C_{P,Y}^{uu}\left(\overline{u_N}(P_f)\begin{bmatrix} G_P^{p,u} & 0\\ 0 & G_P^{n,u}\end{bmatrix}\gamma_5 u_N(P_i) - \frac{m_N(G_A^{p,u} - G_A^{n,u})|\vec{q}|^2}{2m_u(|\vec{q}|^2 + m_\pi^2)}\overline{u_N}(P_f)[\tau_3]\gamma_5 u_N(P_i)\right)\overline{u_e}P_Y u_\mu. \tag{9}$$

In summary, the axial vector and pseudoscalar quark operators could equivalently have been matched at μ_N to an EFT without pions, but with a q^2-dependent "form factor" for the pseudoscalar nucleon operator, and an additional dimension seven derivative operator,

$$\mathcal{O}_{Der,Y}^{NN} = i(\bar{e}\gamma^\alpha P_Y\mu)(\overline{N}\overleftrightarrow{\partial_\alpha}\gamma_5 N), \tag{10}$$

such that $i\langle N(P_f, s')|\bar{N}(x)\overleftrightarrow{\partial_\alpha}\gamma_5 N(x)|N(P_i, s)\rangle = \bar{u}_N^{s'}(P_f)q_\alpha\gamma_5 u_N^s(P_i)e^{-i(P_f-P_i)\cdot x}$. In this extended basis, the nucleon coefficients are

$$\begin{aligned}\widetilde{C}_{A,Y}^{NN} &= G_A^{N,u}C_{A,Y}^{uu} + G_A^{N,d}C_{A,Y}^{dd} + G_A^{N,s}C_{A,Y}^{ss},\\ \widetilde{C}_{Der,Y}^{NN} &= \frac{m_\mu m_N}{(m_\mu^2 + m_\pi^2)}\left(G_A^{N,u} - G_A^{N,d}\right)\left(C_{A,Y}^{uu} - C_{A,Y}^{dd}\right),\\ \widetilde{C}_{P,Y}^{NN} &= G_P^{N,u}C_{P,Y}^{uu} + G_P^{N,d}C_{P,Y}^{dd} + G_P^{N,s}C_{P,Y}^{ss}\\ &\quad - \left(\frac{C_{P,Y}^{uu}}{2m_u} - \frac{C_{P,Y}^{dd}}{2m_d}\right)\frac{m_N(G_A^{Nu} - G_A^{Nd})m_\mu^2}{(m_\mu^2 + m_\pi^2)},\\ \widetilde{C}_{T,Y}^{NN} &= G_T^{N,u}C_{T,Y}^{uu} + G_T^{N,d}C_{T,Y}^{dd} + G_T^{N,s}C_{T,Y}^{ss},\\ \widetilde{C}_{V,Y}^{NN} &= G_V^{N,u}C_{V,Y}^{uu} + G_V^{N,d}C_{V,Y}^{dd}\end{aligned} \tag{11}$$

[2] Such two-nucleon contributions, which arise at NLO, have been studied in WIMP scattering [24–26], and recently considered for coherent $\mu \to e$ conversion in [29].

where $\widetilde{C}^{NN}_{Der,Y}$ was evaluated at $q^2 = -m_\mu^2$, and the scalar nucleon coefficients, to which also gluon operator of Eq. (2) contributes, are given in [15].

To obtain the $\mu \to e$ conversion rate, the expectation values of the nucleon operators in the nucleus are required. This is discussed in the next section. We were unable to find nuclear expectation values of the tensor and pseudoscalar operator, so $\mathcal{O}^{NN}_{P,Y}$ will be neglected, and the tensor included in the scalar and axial operators, as described in Eq. (19).

3 Estimating the SD and SI rate in light nuclei

In Ref. [18] we gave analytic estimates of the SI and SD conversion rates on aluminium. The aim of Sect. 3.1 is to give details of the calculation in the notation of relativistic, second-quantised field theory. The results can then be matched onto the nuclear physics calculations of [14] (for SI conversion), and SD WIMP scattering [24,31–33] (for SD conversion). In Sect. 3.1.3, the estimates are mapped onto the numerical results of KKO [14], and SD conversion in heavier targets is discussed in Sect. 3.2.

3.1 Estimating the SD and SI rate in aluminium

We define the bound state of momentum P_i composed of an aluminium nucleus and a muon in the $1S$ orbital as $\equiv |\mathrm{Al}\mu(P_i)\rangle$. We are interested in the S-matrix element for $\mathrm{Al}\mu(P_i) \to \mathrm{Al}(P_f) + e^-_X(q)$ induced either by the dipole operator (which we discuss later), or by a four-fermion operator $(\overline{e_X}\Gamma_l\mu)(\overline{N}\Gamma_n N)$. To be concrete, we consider the S-matrix element where the nucleon N is a proton:

$$i2\sqrt{2}G_F\widetilde{C}^{pp}_\Gamma\langle \mathrm{Al}(P_f), e(q,s)| \int \mathrm{d}^4y [\overline{\hat{e_X}}(y)\Gamma_l\hat{\mu}(y)] \times[\overline{\hat{p}}(y)\Gamma_n\hat{p}(y)]|\mathrm{Al}\mu(P_i)\rangle \quad (12)$$

where s is the spin of the electron selected by the chiral projector P_X, field operators wear hats, and $\Gamma_n \in \{I, \gamma_5, \gamma^\alpha, \gamma^\beta\gamma_5, \sigma^{\alpha\beta}\}$, $\Gamma_l \in \{I, \gamma^\alpha, \sigma^{\alpha\beta}\}$.

3.1.1 Four-fermion operators

1. A first step is to write the motionless bound state $|\mathrm{Al}\mu(0)\rangle$ as

$$|\mathrm{Al}\mu(\vec{P}_i = 0)\rangle = \sqrt{\frac{2(M_{\mathrm{Al}} + m_\mu)}{4M_{\mathrm{Al}}m_\mu}} \sum_w \int \frac{\mathrm{d}^3k}{(2\pi)^3} \times \widetilde{\psi}_\mu(\vec{k})\,|\mathrm{Al}(-\vec{k})\rangle \otimes |\mu(\vec{k}, w)\rangle \quad (13)$$

where w is the spin of the muon, the square-root prefactor accounts for one- vs. two-body normalisation of states in Lorentz-covariant field theory conventions where states are normalised $\propto \sqrt{2E}$ [34], and $\widetilde{\psi}_\mu(\vec{l}) = \int \mathrm{d}^3z e^{-i\vec{l}\cdot\vec{z}}\psi_\mu(\vec{z})$ is the Fourier transform of the Schrodinger wavefunction $\psi_\mu(\vec{z})$ for a muon in a central potential of charge Z.
For $Z\alpha \ll 1$, the unit-normalised wavefunction, for either spin state, can be approximated [35–37] as

$$\psi_\mu(r,\theta,\phi) \simeq \frac{[m\alpha Z]^{3/2}}{\sqrt{\pi}} e^{-Z\alpha m r}. \quad (14)$$

We approximate the outgoing electron as a free particle (plane wave), which should be acceptable for an aluminium target. For heavy nuclei, the Dirac equation for the electrons outgoing in the field of the nucleus should be solved [13], allowing to express the electron as a superposition of free states. This approach was followed in KKO [14].
2. In the same non-relativistic bound state formalism (see e.g., Appendix B of [32] for more details), the aluminium nucleus, of spin J_A, can be written as a bound state composed of a proton of spin t, with another state M_1 of mass M_1 and spin J_M containing $Z-1$ protons and $A-Z$ neutrons:

$$\langle \mathrm{Al}(P_f), J_A| = \sqrt{\frac{2M_{\mathrm{Al}}}{4M_1m_p}} \sum_{t,J_M} \int \frac{\mathrm{d}^3l}{(2\pi)^3} \tilde{f}^*_p(\vec{l}, t, J_M, J_A) \times \langle M_1(-\vec{l} + M_1\vec{v}_f), J_M| \times \langle p(\vec{l} + m_p\vec{v}_f), t| \quad (15)$$

where $\tilde{f}_p(\vec{l}, t, J_M, J_A)$ is the Fourier transform of the (unknown) wavefunction of the proton in the potential of M_1, and $P_f = (M_{\mathrm{Al}}, M_{\mathrm{Al}}\vec{v}_f)$.
3. The fermion operators can be expanded as [34]

$$\hat{\mu}(y) = \sum_w \int \frac{\mathrm{d}^3p}{(2\pi)^3} \frac{1}{\sqrt{2E}} \left(\hat{a}^w_p u^w_p e^{-ip\cdot y} + \hat{b}^{w\dagger}_p v^w_p e^{ip\cdot y}\right) \quad (16)$$

and act on states as $\hat{\mu}(y)|\vec{k}, w\rangle = u^w_k e^{-ik\cdot y}|0\rangle$, where the spinors are normalised as $u^\dagger_k u_k = 2k_0$. The S-matrix element of Eq. (12) can then be evaluated as

$$i(2\pi)^4\delta^4(P_i - P_f - q)\,2\sqrt{2}G_F\widetilde{C}^{pp}_\Gamma \frac{M_{\mathrm{Al}}}{m_p\sqrt{2m_\mu}} \times \sum_{p\in\mathrm{Al}}\sum_{\mathrm{spins}} \int \mathrm{d}^3x \psi_\mu(\vec{x})|f_p(\vec{x}, J_A, J_M, t)|^2 \times e^{-i\vec{q}\cdot\vec{x}}(\overline{u}^s_e\Gamma u^w_\mu)(\overline{u}^o_p\Gamma u^t_p) \quad (17)$$

where the spinors subscripts are particle names rather than momenta, and $P_i \simeq (M_{\mathrm{Al}} + m_\mu, \vec{P}_i)$, $P_f \simeq (M_{\mathrm{Al}}, \vec{P}_f)$. To obtain this approximation, the states were taken to be non-relativistic, the wavefunctions expressed

in position space, the proton wavefunction was assumed independent of the proton spin, and the dependence of spinors on three-momenta was neglected in many integrals. Notice the $M_{\rm Al}/m_p$ enhancement factor that arises automatically for both spin-dependent and spin-independent interactions, and that the usual $(2\pi)^4\delta^4(P_i - P_f - q)$, which accounts for four-momentum conservation, appears despite that there is a spatial integral over the nucleus. In the following, we drop the spin indices in the nucleon distribution in the nucleus $|f_N|^2$.

4. The leptonic spinor contraction is independent of $\vec{x}$ and can be factored out of the spatial integral in Eq. (17). In light nuclei such as aluminium, the muon wavefunction can also be factored out [10], because the muon wavefunction decreases on the scale $\sim 1/(Z\alpha m_\mu)$, which is larger than the radius of the aluminium nucleus, given in [38] as $\lesssim 6$ fm. On the other hand, the first zero of the electron plane wave (the $e^{-i\vec{q}\cdot\vec{x}}$ of Eq. (17)) would occur at $r \sim \pi/(m_\mu) \sim 6$ fm.
5. The nucleon spinor contractions, in the non-relativistic limit, can be written (see Eq. (47) of [39]) thus:

$$\begin{aligned}
\overline{u}^o_N(P_f)u^t_N(P_i) &\to 2m_N\delta^{ot},\\
\overline{u}^o_N(P_f)\gamma_5 u^t_N(P_i) &\to 2\vec{q}\cdot\vec{S}_N,\\
\overline{u}^o_N(P_f)\gamma^\alpha u^t_N(P_i) &\to 2m_N\delta^{ot}\delta^{\alpha 0},\\
\overline{u}^o_N(P_f)\gamma^j\gamma_5 u^t_N(P_i) &\to 4m_N S^j_N,\\
\overline{u}^o_N(P_f)\sigma_{ik}u^t_N(P_i) &\to 4m_N\epsilon_{ikj}S^j_N,\\
\overline{u}^o_N(P_f)\sigma^{0k}u^t_N(P_i) &\to iq^k,
\end{aligned} \tag{18}$$

where the spin vector of the nucleon is defined as $2\vec{S}_N = u^\dagger_N\vec{\Sigma}u_N/2E_N$, and the rotation generator $S^{ij} = \frac{i}{4}[\gamma^i,\gamma^j] = \frac{1}{2}\epsilon^{ijk}\Sigma^k$. The momentum transfer $q = P_i - P_f$ has been neglected, except in the case of the pseudoscalar, where the leading term is $\mathcal{O}(\vec{q}\cdot\vec{S}_N)$, and in the case of the tensor, where the there is a "spin-independent" contribution $\propto \vec{q}$.

These spinor identities allow the tensor interaction involving nucleons to be absorbed into the scalar and axial vector coefficients. Following [18], we define

$$\begin{aligned}
\widetilde{C}'^{NN}_{S,Y} &= \widetilde{C}^{NN}_{S,Y} + 2\frac{m_\mu}{m_N}\widetilde{C}^{NN}_{T,Y},\\
\widetilde{C}'^{NN}_{A,Y} &= \widetilde{C}^{NN}_{A,Y} + 2\widetilde{C}^{NN}_{T,X}
\end{aligned} \tag{19}$$

where in both cases the factor 2 arises from the two anti-symmetric contributions of the tensor, the unprimed $\widetilde{C}$s are defined in Eq. (11), $X, Y \in \{L, R\}$, and $X \neq Y$ because only operators with electrons of the same chirality can interfere. Notice that there is an error in [18], where is written $\widetilde{C}^{NN'}_{A,Y} = \widetilde{C}^{NN}_{A,Y} + 2\widetilde{C}^{NN}_{T,Y}$.

6. It remains to evaluate the expectation value of the nucleon currents in the nucleus.

(a) In the case of the scalar or vector operators, the matrix element of Eq. (17) becomes

$$\begin{aligned}
\mathcal{M} = {} & 2\sqrt{2}G_F\widetilde{C}^{pp'}_{S,V}\frac{2M_{\rm Al}}{\sqrt{2m_\mu}}\psi_\mu(0)\\
& \times\sum_{p\in A}\int {\rm d}^3x|f_p(r)|^2\frac{\sin(qr)}{qr}\\
& \times\sum_{s,r}\begin{cases}(\overline{u}^s_e u^r_\mu) & \text{scalar},\\ (\overline{u}^s_e\gamma^0 u^r_\mu) & \text{vector},\end{cases}
\end{aligned} \tag{20}$$

where the sum over protons in the nucleus will give a factor Z, we drop the spin indices because the sum and average give 1, and assume a spherically symmetric nucleon distribution $|f_p(r)|^2$ in the nucleus, which allows one to replace[3] $e^{-i\vec{q}\cdot\vec{x}} \to \frac{\sin(qr)}{qr}$. The "form factors"

$$F_N(m_\mu) = \int {\rm d}^3x|f_N(r)|^2\frac{\sin(m_\mu r)}{m_\mu r} \tag{21}$$

are defined in Eqs. (29) and (30) of [14]: $F_p(m_\mu) \sim 0.53$ for Al, and ~ 0.35 for Ti.

(b) The expectation value of the axial current in aluminium ($A = 27$, $Z = 13$, $\vec{J}_{\rm Al} = 5/2$) was calculated by Engel et al. [33] and Klos et al. [24] using the shell model. In the zero momentum transfer limit, where the spin-expectation values S^A_N are defined by

$$\sum_{N\in A}\int {\rm d}^3x|f_N(\vec{x})|^2(\overline{u}_N\gamma^k\gamma_5 u_N) = 4m_N S^A_N\frac{J^k_A}{|J_A|}, \tag{22}$$

they obtain $S^{\rm Al}_n = 0.0296$, $S^{\rm Al}_p = 0.3430$. (J^k_A is a quantum mechanical operator, to be evaluated in the ground state of the nucleus A).

At finite momentum transfer, references [24,33] include the nucleon axial vector operators $\mathcal{O}^{NN}_{A,X}$ and the pion exchange operator $\mathcal{O}^{NN}_{Der,X}$, in the combination induced by axial vector quark operators. The various terms in the matrix-element-squared have different spin sums, so the finite momentum transfer correction depends on $\widetilde{C}^{pp'}_{A,X}$ and $\widetilde{C}^{nn'}_{A,X}$, and is quoted as a multiplicative factor $S_A(m_\mu)/S_A(0)$ in the rate (see Eq. (26)). Neglecting $S^{\rm Al}_n \ll S^{\rm Al}_p$, the results of Engel et al. for aluminium give [33]

$$\begin{aligned}
S_{\rm Al}(k) \propto {} & (0.31500480 - 1.857857y\\
& + 4.86816y^2 - 5.422770y^3)
\end{aligned} \tag{23}$$

[3] Recall that a plane wave can be expanded on spherical harmonics as $e^{iqz} = \sum_{\ell=0}^\infty i^\ell\sqrt{(4\pi)(2\ell+1)}\,j_\ell(qr)Y^0_\ell(\theta)$, and $Y^0_0(\theta) = 1/\sqrt{4\pi}$.

where $y = (m_\mu b/2)^2$ and b =1.73 fm. This gives $S_{\rm Al}(m_\mu)/S_{\rm Al}(0) = 0.29$.

(c) At zero momentum transfer, the nuclear expectation value of tensor operators $\mathcal{O}^{NN}_{T,X}$ is proportional to that of axial vector operators, as accounted for in Eq. (19). However, at finite momentum transfer, there is no pion exchange contribution for the tensor operator (while pion exchange induces $\mathcal{O}^{NN}_{Der,X}$ in the presence of the axial vector quark operators), so the redefinition of Eq. (19) is not valid. Indeed, the tensor and axial vector operators are distinct at finite momentum transfer.
However, we did not find nuclear calculations of SD scattering on aluminium mediated by the tensor operator. We can try to estimate the error from using the axial results for the tensor: at $q^2 = -m_\mu^2$, the pion exchange contribution to the matrix element in Eq. (8) is comparable to the four-fermion contact interaction. Also, the finite momentum transfer suppressions of the axial and scalar rates on aluminium are comparable ($S_{\rm Al}(m_\mu)/S_{\rm Al}(0) \simeq |F_N(m_\mu)|^2$), despite that one might expect the oscillations of the electron wavefunction to suppress the SD rate more than the SI rate, because spin-carrying nucleons are likely to be at large radii. So we interpret this as follows: the axial matrix element is amplified by a factor ~ 2 at $q^2 = -m_\mu^2$ (due to the pion), and suppressed by an extra factor $\sim 1/2$ (as compared to the scalar matrix element) due to the oscillations of the electron wavefunction, and we estimate that the identification of Eq. (19) could overestimate the tensor contribution to the branching ratio by a factor $\sim 2 \to 4$ (depending on whether the pseudoscalar and axial matrix elements interfere).

(d) The pseudoscalar operator $\mathcal{O}^{NN}_{P,X}$ is proportional to the nucleon spin, is only present at finite momentum transfer, and at $q^2 = -m_\mu^2$, is enhanced by a pion exchange contribution of comparable magnitude. Since the magnitude of the pseudoscalar spinor contraction in Eq. (18) is suppressed with respect to the axial vector by $\sim m_\mu/2m_N$, its contribution to the SD branching ratio could be $\sim m_\mu^2/4m_N^2 \times$ the axial vector contribution. However, the identification $\widetilde{C}''^{NN}_{A,Y} = \widetilde{C}'^{NN}_{A,Y} + \frac{m_\mu}{2m_N}\widetilde{C}^{NN}_{P,X}$ does not work, because the spin sums suppress the axial–pseudoscalar interference term. A dedicated nuclear calculation would seem required for both the pseudoscalar and the tensor operators.

7. To obtain the matrix-element-squared, the lepton spinor part can be evaluated by Dirac traces. Then to perform the nuclear spin sums in the SD case, the identity

$$\frac{1}{(2J_\mu+1)(2J_A+1)}\sum_{\rm spins}\sum_{k,i}\langle J_\mu|\hat{J}^k_\ell|J'_e\rangle\langle J'_e|\hat{J}^i_\ell|J_\mu\rangle \times\langle J'_A|\hat{J}^k_A|J_A\rangle\langle J_A|\hat{J}^i_A|J'_A\rangle = \frac{1}{3}J_\mu(J_\mu+1)J_A(J_A+1) \tag{24}$$

can be used.

8. Finally, the conversion rate is obtained:

$$\Gamma = \frac{1}{2M_{\rm Al}}\int {\rm d}\Pi\overline{|\mathcal{M}|}^2 = \frac{m_\mu}{8M^2_{\rm Al}\pi}\overline{|\mathcal{M}|}^2$$

where $\overline{|\mathcal{M}|}^2$ is averaged over the incident spins, and dΠ gives the integration over the final-state phase space of the nucleus and electron.

These steps give an analytic estimate for the four-fermion contributions to the SI conversion rate on a nucleus of atomic number A and charge Z:

$$\frac{\Gamma_{\rm SI}}{\Gamma_{\rm capt}} = 2B_0|Z(\widetilde{C}'^{pp}_{S,L} + \widetilde{C}^{pp}_{V,R} + 2eC_{D,L})F_p(m_\mu) + (A-Z)(\widetilde{C}'^{nn}_{S,L} + \widetilde{C}^{nn}_{V,R})F_n(m_\mu)|^2 + \{L \leftrightarrow R\}. \tag{25}$$

where the F_N are defined in Eq. (21) and related to the overlap integrals of KKO in (34), the contribution of the dipole operator (estimated in Sect. 3.1.2) was also included, and

$$B_0 = \frac{G_F^2 m_\mu^5}{\Gamma_{\rm capt}\pi^2}(Z\alpha)^3 \simeq \begin{cases} 0.310 \text{ Al } (Z=13), \\ 0.438 \text{ Ti } (Z=22), \end{cases}$$

where $\Gamma_{\rm capt}$ is the rate for the standard model process of muon capture [14,40]. Similarly, the SD conversion rate on a nucleus of atomic number A, charge Z and spin J_A is

$$\frac{\Gamma_{\rm SD}}{\Gamma_{\rm capt}} = 8B_0\frac{J_A+1}{J_A}\left|S^A_p\widetilde{C}'^{pp}_{A,L} + S^A_n\widetilde{C}'^{nn}_{A,L}\right|^2\frac{S_A(m_\mu)}{S_A(0)} + \{L \leftrightarrow R\}, \tag{26}$$

where the spin-expectation values S^A_N and the finite momentum transfer correction $S_A(k)$ are given for aluminium at Eq. (23).

3.1.2 The dipole

In the case of the dipole operator of Eq. (2), the S-matrix element can be written

$$i\frac{2\sqrt{2}G_F}{\sqrt{2m_\mu}}C_{D,Y}m_\mu\langle e(q,s)|\int {\rm d}^4y 2(\overline{\hat{e_X}}(y)\sigma^{0i}\cdot \times E_i(y)P_Y\hat{\mu}(y))|\mu(q)\rangle \tag{27}$$

$$= i\frac{2\sqrt{2}G_F}{\sqrt{2m_\mu}}C_{D,Y}m_\mu 2\pi\delta(E_e - m_\mu) \times \int \mathrm{d}^3y e^{-i\vec{q}\cdot\vec{y}}\psi_\mu(\vec{y})2(\overline{u_e}\sigma^{0i}\cdot E_i(y)P_Y u_\mu(y)) \quad (28)$$

$$\equiv i2\pi\delta(E_e - m_\mu)\widetilde{\mathcal{M}}, \quad \widetilde{\mathcal{M}} = \frac{2\sqrt{2}G_F}{\sqrt{2m_\mu}}2C_{D,Y}m_\mu \times \int \mathrm{d}\Omega r^2\mathrm{d}r\frac{\sin m_\mu r}{m_\mu r}\psi_\mu(r)(\overline{u_e}\sigma^{0i}P_Y u_\mu)E_i(r) \quad (29)$$

where the 2 under the integral is to account for $E_i = F_{0i} = F_{i0}$, and the magnitude of the radial electric field induced by the nucleus is [14]

$$E(r) = \frac{Ze}{r^2}\int_0^r r'^2|f_p(r')|^2\mathrm{d}r'. \quad (30)$$

To estimate the dipole matrix element analytically, we suppose that the electric field only contributes at radii within the first zero of the electron wavefunction r_e, because outside the rapid oscillation of the electron wavefunction gives an approximate cancellation in $\mathcal{M}$. The muon wavefunction is approximately constant at such radii. The radius of the aluminium nucleus is comparable to r_e, but if we nonetheless approximate the nucleon distribution $|f_p(r)|^2$ as a constant for $r < r_e$, we obtain

$$E(r) \simeq \frac{Zer}{3}|f_p(r)|^2, \quad \widetilde{\mathcal{M}} \simeq \frac{2\sqrt{2}G_F}{\sqrt{2m_\mu}}2C_{D,Y}m_\mu\psi_\mu(0) \times \int \mathrm{d}\Omega\frac{r^3\mathrm{d}r}{3}|f_p(r)|^2\frac{\sin m_\mu r}{m_\mu r}(\overline{u_e}\sigma^{0i}P_Y u_\mu)Ze\hat{r}_i \quad (31)$$

where $\hat{r}$ is a radial unit vector.

The "matrix element" $\widetilde{\mathcal{M}}$ neglects recoil of the nucleus, so the final-state phase space in the rate is only one-body, and we reproduce the analytic estimate of [14] for light nuclei ($D \sim 8eS^p$ given above Eq. (29) of [14]):

$$\mathrm{BR}_{\mathrm{SI}} = \overline{|\widetilde{\mathcal{M}}|^2}\frac{m_\mu}{2\pi} = \frac{8G_F^2m_\mu^5}{\pi^2\Gamma_{\mathrm{capt}}}(\alpha Z)^3|ZeC_{D,Y}F_p(m_\mu)|^2. \quad (32)$$

This estimate uses $\int r^3\mathrm{d}r/3 \simeq \int r^2\mathrm{d}r$, and it applies in the absence of other contributions; the dipole coefficient sums with the scalar and vector coefficients in the amplitude, as given in Eq. (25).

3.1.3 Comparing to KKO

This section compares our estimates to the more exact formulae of [14] (KKO). Our estimates use a solution of the Schrödinger equation for the muon, a plane wave for the electron, and chiral γ-matrices. KKO solve the Dirac equation in the potential of the nucleus, both for the electron and muon, use Bjorken and Drell γ-matrix conventions, and give the branching ratio as

$$\mathrm{BR}(A\mu \to Ae) = \frac{32G_F^2m_\mu^5}{\Gamma_{\mathrm{cap}}}\Big[\big|\widetilde{C}_{V,R}^{pp}V^{(p)} + \widetilde{C}_{S,L}^{\prime pp}S^{(p)} + \widetilde{C}_{V,R}^{nn}V^{(n)} + \widetilde{C}_{S,L}^{\prime nn}S^{(n)} + C_{D,L}D\big|^2 + \{L \leftrightarrow R\}\Big] \quad (33)$$

where Γ_{cap} is the rate for the muon to transform to a neutrino by capture on the nucleus (see [14,40]), and the nucleus- and nucleon-dependent "overlap integrals" $V_X^{(N)}$, $S_X^{(N)}$, $D^{(N)}$ correspond to the integral over the nucleus of the lepton wavefunctions and the appropriate nucleon density (vector, scalar, electric field for the dipole operator; the definitions and numerical values are given in KKO [14]). The numerical coefficient in Eq. (33) differs from the result given in KKO, because $4\widetilde{C}|_{\mathrm{here}} = \tilde{g}|_{\mathrm{KKO}}$.

Our unit-normalised nuclear density $|f_N(r)|^2$ can be identified with the similarly normalised density $\rho_N(r)$ of KKO [14]. Our Schrödinger approximation for the muon wavefunction can be identified to the upper component (in Bjorken and Drell γ conventions) of the Dirac wavefunction obtained by [14]. Then the normalisation conventions of Eqs. (5) and (7) of [14] identify

$$\psi_\mu(r,\theta,\phi) \leftrightarrow \frac{g_\mu(r)}{\sqrt{4\pi}}.$$

In the limit of massless electron, the upper (g_e) and lower components (if_e) of the electron wavefunction of [14] are comparable. The electron normalisation condition given in Eq. (8) of [14] then implies that we can identify our electron plane wave as

$$if_e = g_e(r) \leftrightarrow \sqrt{2}\frac{\sin m_\mu r}{r} \leftrightarrow \sqrt{2}m_\mu e^{-i\vec{k}\cdot\vec{r}}.$$

In the approximation where the muon wavefunction is constant in the nucleus, the overlap integrals of [14] can be identified to our approximations as

$$S^{(p)}, V^{(p)} \to \frac{m_\mu|\psi_\mu(0)|}{4\sqrt{\pi}}Z\int \mathrm{d}^3x e^{-i\vec{k}\cdot\vec{x}}|f_p|^2$$
$$S^{(n)}, V^{(n)} \to \frac{m_\mu^{5/2}(Z\alpha)^{3/2}}{4\pi}(A-Z)\int \mathrm{d}^3x e^{-i\vec{k}\cdot\vec{x}}|f_n|^2, \quad (34)$$

as given in Eqs. (29)–(31) of KKO.

3.2 Spin-dependent conversion in other light nuclei

In this section we consider how the estimates of the previous section could be applied to other nuclei. Recall that light nuclei are interesting for SD detection, because the SD rate

is relatively suppressed by $1/A^2$ compared to the SI rate: the ratio $\Gamma_{\rm SD}/\Gamma_{\rm SI}$ is largest for light nuclei.

The matrix element given in Eq. (17) for SD $\mu \to e$ conversion contains the integral of the axial current over the nucleus, weighted by the lepton wavefunctions. In the case of light nuclei ($Z \lesssim 20$), as discussed in the previous section, the muon wavefunction can be taken constant in the nucleus, and the electron can be treated as a plane wave. This allows one to use the results of nuclear calculations [31] of matrix elements for spin-dependent WIMP scattering at finite momentum transfer. The zero momentum transfer matrix elements (spin-expectation values; see Eq. (22)), have been calculated for a wide variety of nuclei [41], and finite momentum transfer results also been obtained for some nuclei [42]. For $\mu \to e$ conversion in heavier nuclei, a dedicated nuclear calculation would be required to obtain the expectation values of the SD operators weighted by the lepton wavefunctions.

An interesting light nucleus for SD $\mu \to e$ conversion could be titanium ($Z = 22$),[4] because it has isotopes with and without spin, so targets of different isotopic abundances could allow one to distinguish SD from SI operators. Titanium has a spin-zero isotope with $A = 48$ and 74% natural abundance [43], an isotope with $A = 47$, $J = 5/2$, 7.5% abundance, and another isotope with $A = 49$, $J = 7/2$, 5.4 % abundance. These natural abundances of more than 5 % are large enough to make sufficiently enriched sample targets.

In the odd group model, Engel and Vogel [44] obtained spin-expectation values $S_n^{\rm Ti,47} = 0.21$, $S_p^{\rm Ti,47} = 0$, and $S_n^{\rm Ti,49} = 0.29$, $S_p^{\rm Ti,49} = 0$. Unfortunately, we were unable to find finite momentum transfer corrections to the spin-expectation values in titanium. However, we observe that in aluminium, the SI and SD form factors are comparable: $0.28 = |F_p(m_\mu)|^2 \approx S_{\rm Al}(m_\mu)/S_{\rm Al}(0) = 0.29$. A similar relation appears to hold [14,42] for fluorine, where $|F_n(m_\mu)|^2 \approx S_{\rm Fl}(m_\mu)/S_{\rm Fl}(0) \approx 0.36$. This suggests that, for light nuclei, the spin-expectation-squared at $|\vec{q}|^2 \neq 0$ (that is, $S_A(m_\mu)$), is similar to the square of the spin-expectation value at zero momentum transfer, multiplied by the square of the SI $|\vec{q}|^2 \neq 0$ form factor. Or taking the square root:

$$\begin{aligned}&\sum_{p\in A}\int {\rm d}^3x |f_p(\vec{x})|^2 e^{-i\vec{q}\cdot\vec{x}}(\overline{u}_p\gamma^k\gamma_5 u_p)\\ &\quad\approx \sum_{p\in A}\int {\rm d}^3y |f_p(\vec{y})|^2(\overline{u}_p\gamma^k\gamma_5 u_p)\\ &\quad\times \int {\rm d}^3z |f_p(\vec{z})|^2 e^{-i\vec{q}\cdot\vec{z}}.\end{aligned} \tag{35}$$

[4] titanium was used as a target by SINDRUMII [3–5], who set an upper bound ${\rm BR}(\mu{\rm Ti}\to e{\rm Ti}) < 4.3\times 10^{-12}$.

So we apply this approximation to titanium and estimate $S_{\rm Ti}(m_\mu)/S_{\rm Ti}(0) \approx 0.12$.

4 Parametric expansions and uncertainties

Once $\mu \to e$ conversion is observed, the aim will be to determine (or constrain) as many operator coefficients as possible. This would require at least as many "independent" observations as operators, where observations are independent if, in spite of uncertainties, they depend on a different combination of coefficients. So the purpose of this section, is to estimate the uncertainties in relating the conversion rate to operator coefficients.

The inputs for this calculation (equivalently, the theoretical parameters to be extracted from data) are the coefficients of either the quark operators (see Eq. (1)), or of the nucleon operators [see Eqs. (11) and (19)], in both cases at the experimental scale μ_N. So uncertainties associated to the renormalisation group evolution from the new physics scale to the experimental scale are not considered. In the remainder of this paper, we will sometimes use the quark operator basis, and sometimes the nucleon basis. As discussed in point 1 below, there are significant uncertainties in some of the $\{G_O^{N,q}\}$, which are required to extract the coefficients of the quark operators, but can be avoided by using the nucleon operators.

1. There are uncertainties in some of the matching coefficients that relate quark to hadron operators (see Eq. (6) and Appendix A). The $G_V^{N,q}$ are from charge conservation, so should be exact. For the axial and scalar coefficients, the determinations from data (see Eq. (62)) and from the lattice (63, 65) are quoted with smaller uncertainties than their differences (this is especially flagrant for the $G_S^{N,q}$, whose lattice and data values differ by 30–50%, and which are both quoted with $\lesssim$ 10% uncertainties). First, it can be hoped that these discrepancies will be reduced in the future. Secondly, in some models (or equivalently, for some choices of coefficients), these factors can be cancelled by taking ratios. Finally, if we are only interested in discriminating SD from SI contributions to the rate, this distinction exists at the nucleon level, so the matching to quark operators is not required.
2. The lepton interactions with nucleons are calculated at leading order (LO) in χPT. At NLO, pion loops arise as well as processes with two nucleons in the initial and final states which exchange a pion that interacts with the leptons. For the case of WIMP scattering, such NLO contributions for the scalar quark operator have been discussed [25,26,45] and reference [25] estimates them to be a higher order effect ($\lesssim$ 10%), provided there are no can-

cellations among the LO contributions. The two-nucleon contributions were also calculated to be unexpectedly small for WIMP scattering on few-nucleon nuclei [46]. However, after this manuscript was completed, appeared a study of the $\mu \to e$ conversion rate mediated by the scalar and vector interactions [29], where the authors estimate that the NLO effects associated to pion exchange between two nucleons can reduce the scalar matrix element by $20 \to 30\%$ (NLO corrections vanish for the vector). We will account for these nucleon/χPT uncertainties by including them in the uncertainties in the overlap integrals.

3. The $\mu \to e$ conversion matrix element, expressed as a function of nucleon operator coefficients, relies on many perturbative expansions, among which an expansion in the finite momentum transfer $|\vec{q}|^2 = m_\mu^2$. Naively such corrections are $\mathcal{O}(m_\mu^2/m_N^2)$ (so negligible); however, in practise there are various effects which are not so suppressed. First, the finite momentum transfer gives a significant suppression of the matrix element. In our analytic approximations, where the muon is at rest and the electron momentum $\vec{k} = \vec{q}$, this is encoded in the form factors F_N (see Eq. (21)), which are $\sim 0.2 \to 0.7$. KKO include this effect more accurately, by solving the Dirac equation for the leptons. Secondly, finite momentum transfer effects can change the nucleon and lepton spinor algebra. This is discussed for dark matter in [32,39] and gives the $\mathcal{O}(m_\mu/m_N)$ contribution of the tensor to the scalar coefficient given in Eq. (19). We include this correction, because the tensor operator at zero momentum transfer contributes to the SD matrix element (suppressed by $1/A$), whereas this (m_μ/m_N)-suppressed contribution gains a relative factor A because it contributes to the SI matrix element. The ratio of these contributions to the conversion rate is estimated in Appendix B. Finally, pion exchange becomes relevant at $|\vec{q}|^2 = m_\mu^2$ for the axial vector and pseudoscalar operators (see Eqs. (8) and (9)), and it is included in the nuclear matrix elements of [33], which we use for the axial vector in aluminium. Pion contributions at $|\vec{q}| \neq 0$ to the SI rate are discussed above. We hope that these are the dominant finite momentum transfer corrections, such that any other effects are negligible ($< 10\%$) corrections.
4. In our calculation of the SD matrix element, the velocity of the initial muon was neglected. This may seem doubtful, by analogy with the extended basis of WIMP scattering operators constructed in [32], because these authors expand in both the momentum transfer between the WIMP and nucleon, and the incoming velocity difference. However, in our case, the muon velocity is parametrically smaller: writing the binding energy of the $1s$ state as $\pi Z\alpha m_\mu \sim m\vec{v}^2$, gives $|\vec{v}| \sim \sqrt{Z\alpha}$. We neglect any effects related to this velocity.
5. There could be nuclear uncertainties in the SI overlap integrals S^N, V^N, D, in addition to the effects discussed in point 2 above. These were estimated by [14] to be $\sim$ a few % in most cases, $\lesssim 10\%$ in the case of some heavier nuclei.

Consider first the uncertainty on the SI rate, because, when $\mu \to e$ conversion is observed in a nucleus with spin, the SD conversion rate can only be observed, if it is larger than the uncertainty in the ubiquitous A^2-enhanced SI rate. The uncertainty in $\Gamma_{\rm SI}$, written as a function of the quark operator coefficients $C_{O,X}^{qq}$, would arise from the $G_O^{N,q}$, from the overlap integrals S^N, V^N, D of [14], and from NLO contributions in χPT:

$$\frac{\delta\Gamma_{\rm SI}}{\Gamma_{\rm SI}}(C_{O,X}^{qq}) \simeq 2\Bigg(\sum_{X=L,R}\frac{|F_X|}{|F_L|^2+|F_R|^2}\Big(C_{S,X}^{qq}S^N\delta G_S^{N,q} + \widetilde{C}_{S,X}^{NN}[\delta S^N]_{\rm NLO}\Big) + \frac{\delta I_A}{I_A}\Bigg) \tag{36}$$

where $F_L = \widetilde{C}_{V,L}^{NN}V^{(N)} + \widetilde{C}_{S,R}^{\prime NN}S^{(N)} + \widetilde{C}_{D,R}D$, sums on $N \in \{n,p\}$ and $q \in \{u,d,s\}$ are implicit, the gluon contribution to the scalar [15] was neglected, for simplicity a common uncertainty $\frac{\delta I_A}{I_A}$ was assigned to the overlap integrals in nucleus A, except for the effect of neglecting pion exchange between two nucleons [25,29] (discussed in point 2 above), which is parametrised as an uncertainty $[\delta S^N]_{\rm NLO}$ in the scalar overlap integrals. Expressed in this way, the uncertainty depends on the quark coefficients present: for $C_{S,X}^{qq} \gg C_{V,X}^{qq}, C_{D,X}$, the current discrepancies in the determination of the $G_S^{N,q}$ and $[\delta S^N]_{\rm NLO}$ give an $\mathcal{O}(1)$ uncertainty on the conversion rate, whereas if only the $C_{V,X}^{qq}$ and $C_{D,X}$ were present, the rate uncertainty would come from the overlap integrals. The $G_S^{N,q}$ uncertainties can be avoided by expressing the rate in terms of the coefficients of the nucleon Lagrangian; if in addition, $[\delta S^N]_{\rm NLO}/S_N < 10\%$, then the uncertainty in the SI rate comes from the overlap integrals. From the KKO discussion, $2\frac{\delta I_A}{I_A} \lesssim 10\%$ in most cases, $< 20\%$ in all cases. In order to be concrete, we assume in the remainder of this paper that the uncertainty on the SI rate, expressed in terms of the coefficients on nucleons, is $\lesssim 10\%$. This suggests that the SD rate would need to be $\gtrsim 10-20\%$ of the SI rate in order to be observed.

A better sensitivity to the SD rate could be obtained by using isotopes with and without spin as targets: consider for instance, ^{48}titanium (without spin), and ^{47}titanium (with spin), whose SI matrix elements differ by one neutron. Using the analytic approximation of Eq. (25), the ratio of the SI conversion rates, for real coefficients and left-handed electrons, is

$$\frac{\Gamma_{\rm SI}(^{47}{\rm Ti})}{\Gamma_{\rm SI}(^{48}{\rm Ti})} \simeq 1 - 2\frac{\left|(\widetilde{C}'^{nn}_{S,L} + \widetilde{C}^{nn}_{V,R})F_n(m_\mu)\right|}{|Z(\widetilde{C}'^{pp}_{S,L} + \widetilde{C}^{pp}_{V,R} + 2eC_{D,L})F_p(m_\mu) + (A-Z)(\widetilde{C}'^{nn}_{S,L} + \widetilde{C}^{nn}_{V,R})F_n(m_\mu)|} + \cdots \tag{37}$$

where the second term[5] is $\mathcal{O}(1/A)$. The theoretical uncertainty in this ratio will arise from the overlap integrals (equivalently, form factors F_N), so it should be of order $\frac{1}{A}\frac{\delta I_{\rm Ti}}{I_{\rm Ti}} \lesssim 0.002$. This greatly improves the sensitivity to the SD rate, although it is unlikely to allow for as good a sensitivity to SD as SI coefficients, because the SD rate is parametrically suppressed as $1/A^2$, which is $\lesssim \frac{1}{A}\frac{\delta I_{\rm Ti}}{I_{\rm Ti}}$.

Some prospects for distinguishing among SI operators by using different targets will be discussed in Sect. 5.3. For this, the various targets need to probe different combinations of operator coefficients, and this difference needs to be larger than the theoretical uncertainty. In Sect. 5.3, targets are parametrised as vectors in coefficient space, whose components are the overlap integrals (see Eq. (54)), and targets are assumed to probe different combinations of operator coefficients if the angle between the vectors is $\gtrsim 10\% \gtrsim \frac{\delta I_A}{I_A}$. This estimate can be obtained in the 2-dimensional plane of the vectors, where the uncertainty on the angle θ of a point $(I_1 \pm \delta I_1, I_2 \pm \delta I_2)$ is

$$\delta\theta \simeq \frac{\delta I_i}{I_i} \times \frac{I_1 I_2}{I_1^2 + I_2^2} \tag{38}$$

5 Implications of including the SD rate

The aim of this section is to explore the implications of including the SD contribution to $\mu \to e$ conversion. At first sight, it appears to be of limited interest: the ratio of SD to SI rates is

$$\frac{\Gamma_{\rm SD}}{\Gamma_{\rm SI}} \sim \frac{|C_{\rm SD}|^2}{A^2|C_{\rm SI}|^2}$$

so for a SI operator coefficient $C_{\rm SI}$ comparable to $C_{\rm SD}$, the SD contribution to the branching ratio is much smaller than the $\sim 10\%$ theory uncertainty of the SI contribution, estimated in the previous section. Furthermore, as discussed in [18], renormalisation group running between the new physics scale and low energy mixes the tensor and axial vector ("SD") operators to the scalars and vectors, so even in a new physics model that only induces SD operators, their dominant contribution to $\mu \to e$ conversion is via the SI operators that arise due to RG running. This perspective that SD conversion can be ignored is illustrated in Sect. 5.1, where we consider three leptoquark models. They give negligible SD branching ratios, but we explore the prospects of distinguishing them by comparing the SI rates in various nuclei.

The SD conversion rate is nonetheless interesting, because it is an independent observable that can be observed by comparing targets with and without spin. As in the case of dark matter, it is sensitive to different operator coefficients (evaluated at the experimental scale) from the SI process, so it provides complementary information. In Sect. 5.2 we allow for $C_{\rm SD} \gg C_{\rm SI}$ such that the SD rate can be observable, and discuss the constraints that could be obtained from upper bounds on $\mu \to e$ conversion. Finally, in Sect. 5.3, we allow for arbitrary coefficients to all the operators of the nucleon-level Lagrangian, and we explore the prospects for identifying coefficients should $\mu \to e$ conversion be observed.

5.1 Leptoquarks

We consider three possible leptoquark scenarios, each containing an SU(2) singlet leptoquark, whose mass $M \gtrsim$ few TeV respects direct search constraints [47–49], and which has only one coupling to electrons and one to muons. The scenarios are represented by adding to the standard model the following Lagrangians:

$$\begin{aligned}\mathcal{L}_1 &= D^\mu S^\dagger D_\mu S + M^2 S^\dagger S + [\lambda_R^*]_{eu}\bar{e}u^c S \\ &\quad + [\lambda_R^*]_{\mu u}\bar{\mu}u^c S + h.c., \end{aligned} \tag{39}$$

$$\begin{aligned}\mathcal{L}_2 &= D^\mu S^\dagger D_\mu S + M^2 S^\dagger S + [\lambda_L^*]_{\mu d}\bar{\ell}_\mu i\tau_2 q^c_{L,u} S \\ &\quad + [\lambda_R^*]_{eu}\bar{e}u^c S + h.c., \end{aligned} \tag{40}$$

$$\begin{aligned}\mathcal{L}_3 &= D^\mu \tilde{S}^\dagger D_\mu \tilde{S} + \widetilde{M}^2 \tilde{S}^\dagger \tilde{S} + [\tilde{\lambda}^*]_{ed}\bar{e}d^c \tilde{S} \\ &\quad + [\tilde{\lambda}^*]_{\mu d}\bar{\mu}d^c \tilde{S} + h.c., \end{aligned} \tag{41}$$

where D^μ is the appropriate covariant derivative of QCD and QED. At the leptoquark mass scale, we match these scenarios onto the SM extended by QED*QCD invariant operators, which mediate $\mu \to e$ conversion. The coefficients and operators are given in Table 1.

In each scenario, we translate the coefficients down to the experimental scale $\mu_N = 2$ GeV via an approximate analytic solution to the one-loop RGEs of QED and QCD [19,20]:

$$C_I(\mu_N) \simeq C_J(M)\lambda^{a_J}\left(\delta_{JI} - \frac{\alpha_e \widetilde{\Gamma}^e_{JI}}{4\pi}\log\frac{M}{\mu_N}\right) \tag{42}$$

where $\lambda = \frac{\alpha_s(M)}{\alpha_s(\mu_N)} \simeq 1/3$ for $M =$ TeV, and I, J represent the super- and subscripts which label operator coefficients. The a_I describe the QCD running and are only non-zero for scalars and tensors. We suppose five quark flavours for the

[5] Since ^{47}Ti and ^{48}Ti only differ by one neutron, there would be no $\mathcal{O}(1/A)$ term if the CLFV operators only involved protons or the dipole.

Table 1 Lepton flavour-changing operators induced in the leptoquark scenarios of Eqs. (39)–(41). The coefficients are given at the leptoquark mass scale M, in the basis of Sect. 2

	Operators	Coefficients at M
$\mathcal{L}_1$	$-\frac{[\lambda_R]^*_{eu}[\lambda_R]_{\mu u}}{M^2}(\overline{e_R}u^c)(\overline{u^c}\mu_R) = \frac{[\lambda_R]^*_{eu}[\lambda_R]_{\mu u}}{2M^2}(\overline{e_R}\gamma^\alpha\mu_R)(\overline{u}\gamma_\alpha P_R u)$	$C^{uu}_{V,R} = C^{uu}_{A,R} = \frac{[\lambda_R]^*_{eu}[\lambda_R]_{\mu u}}{4M^2}$
$\mathcal{L}_2$	$-\frac{[\lambda_R]^*_{eu}[\lambda_L]_{\mu u}}{M^2}(\overline{e_R}u^c)(\overline{u^c}\mu_L) = \frac{[\lambda_R]^*_{eu}[\lambda_L]_{\mu u}}{2M^2}\left((\overline{e_R}P_L\mu)(\overline{u}P_L u) + \frac{1}{4}(\overline{e_R}\sigma P_L\mu)(\overline{u}\sigma P_L u)\right)$	$C^{uu}_{S,L} = 2C^{uu}_{T,L} = \frac{[\lambda_R]^*_{eu}[\lambda_L]_{\mu u}}{4M^2}$
$\mathcal{L}_3$	$-\frac{[\tilde{\lambda}]^*_{ed}[\tilde{\lambda}]_{\mu d}}{\widetilde{M}^2}(\overline{e_R}d^c)(\overline{d^c}\mu_R) = \frac{[\tilde{\lambda}]^*_{ed}[\tilde{\lambda}]_{\mu d}}{2\widetilde{M}^2}(\overline{e_R}\gamma^\alpha\mu_R)(\overline{d}\gamma_\alpha P_R d)$	$C^{dd}_{V,R} = C^{dd}_{A,R} = \frac{[\tilde{\lambda}]^*_{ed}[\tilde{\lambda}]_{\mu d}}{4\widetilde{M}^2}$

running, which gives $a_I = \frac{\Gamma^s_{II}}{2\beta_0} = \{-\frac{12}{23}, \frac{4}{23}\}$ for $I = S, T$. Γ^e is the one-loop QED anomalous dimension matrix, $\widetilde{\Gamma}^e$ is this matrix with an additional factor multiplying the TS and ST entries [50,51] in order to account for the QCD running:

$$\widetilde{\Gamma}^e_{JI} = \Gamma^e_{JI} f_{JI},\ f_{JI} = \frac{1}{1+a_J-a_I}\frac{\lambda^{a_I-a_J}-\lambda}{1-\lambda} = \begin{cases} \frac{23}{7}\frac{\lambda^{16/23}-\lambda}{1-\lambda} & JI = ST, \\ \frac{23}{39}\frac{\lambda^{-16/23}-\lambda}{1-\lambda} & JI = TS, \\ 1 & \text{otherwise.} \end{cases} \tag{43}$$

We neglect the RG mixing out of our operator basis, because it is small: tensor mixing to the dipole is suppressed by light quark masses, and the mixing via the penguin diagram to vector operators $\mathcal{O}^{ff}_{V,X}$ is a few % and does not generate operators interesting to us here. The RG evolution is described in more detail in Appendix C.

This formalism allows one to predict the ratio of SD to SI contributions to the branching ratio for $\mu \to e$ conversion. In aluminium, we find for the three scenarios, taking $M = 1$ TeV:

$$\begin{aligned} \text{for } \mathcal{L}_1: &\quad \frac{\text{BR}_{\text{SD}}}{\text{BR}_{\text{SI}}} \sim 1.5\times 10^{-4}, \\ \text{for } \mathcal{L}_2: &\quad \frac{\text{BR}_{\text{SD}}}{\text{BR}_{\text{SI}}} \sim 4.4\times 10^{-6}, \\ \text{for } \mathcal{L}_3: &\quad \frac{\text{BR}_{\text{SD}}}{\text{BR}_{\text{SI}}} \sim 3.2, \times 10^{-5} \end{aligned} \tag{44}$$

so we see that the SD rate is smaller than the current $\sim$ 10% uncertainties on the SI rate, so cannot be observed in these models. This is as expected, because the leptoquark model imposes the requirement that the tensor/axial coefficients are comparable to the scalar/vector coefficients, so the SD rate is relatively suppressed with respect to the SI rate by $1/(AG_S^{N,q})^2$ for tensor coefficients, and $1/A^2$ for axial vector coefficients.

It is interesting to explore whether the three leptoquark scenarios could be distinguished by comparing the SI rates in various nuclei. We imagine that $\mu \to e$ conversion has been observed in aluminium ($Z_{\text{Al}} = 13$, $A_{\text{Al}} = 27$), the target of the upcoming COMET and Mu2e experiments. We wish to identify alternative target materials, which could allow one to distinguish our leptoquark scenarios.

A simple distinction between the leptoquarks S and $\widetilde{S}$, is that the former couples to u quarks, and the latter to d quarks. To identify an appropriate target (A, Z), where the $\mu \to e$ conversion rates induced by S and $\widetilde{S}$ would be significantly different (subject to the constraint that both reproduced the aluminium observations), we consider the double ratio:

$$\frac{\frac{\Gamma(\text{Al}\mu\to\text{Al}e)}{\Gamma((A,Z)\mu\to(A,Z)e)}\Big|_S}{\frac{\Gamma(\text{Al}\mu\to\text{Al}e)}{\Gamma((A,Z)\mu\to(A,Z)e)}\Big|_{\widetilde{S}}} \simeq \left(\frac{2A_{\text{Al}}-Z_{\text{Al}}}{A_{\text{Al}}+Z_{\text{Al}}}\right)^2\left(\frac{A+Z}{2A-Z}\right)^2 = \left(\frac{2V^{(p)}_{\text{Al}}+V^{(n)}_{\text{Al}}}{V^{(p)}_{\text{Al}}+2V^{(n)}_{\text{Al}}}\right)^2\left(\frac{V^{(p)}_A+2V^{(n)}_A}{2V^{(p)}_A+V^{(n)}_A}\right)^2 \tag{45}$$

where the operator coefficients cancel because we compare two models that each induce a single SI operator. This ratio should differ from 1 by $\gtrsim 20\%$, in order to unambiguously distinguish the S from $\widetilde{S}$, given the $\sim 10\%$ uncertainties on the theory calculation. The first approximate equality in Eq. (45) applies for light nuclei, where the conversion rate can be written as Eq. (25). The second equality uses the KKO conversion rate given in Eq. (33) in terms of the overlap integrals $V^{(N)}$, and it applies for all nuclei.

The continuous green line (with stars) of Fig. 2 is the ratio of $\mu \to e$ conversion rates mediated by S and $\widetilde{S}$, assuming equal operator coefficients. It corresponds to the second fraction in the products appearing in Eq. (45), so the double ratio of Eq. (45) is simply obtained by dividing by the ratio for aluminium. The stars are the light nucleus approximation, the green continuous line is the ratio of overlap integrals. This shows that the approximation is very similar to the numerical results of KKO, and that a target with $Z \gtrsim 40$ could allow one to distinguish the first and third leptoquark scenarios. In the following, we take niobium (Nb, $Z = 41$, $A = 93$) as a $Z \gtrsim 40$ target.

It is also interesting to explore the prospects of distinguishing scalar operators involving u vs. d quarks. So we also plot in Fig. 2, as a dashed red line, the ratio of $\mu \to e$ conversion rates mediated upstairs by $\mathcal{O}^{uu}_{S,X}$ and downstairs by $\mathcal{O}^{dd}_{S,X}$:

$$\frac{\Gamma((A,Z)\mu\to(A,Z)e)\big|_{\mathcal{O}^{uu}_{S,X}}}{\Gamma((A,Z)\mu\to(A,Z)e)\big|_{\mathcal{O}^{dd}_{S,X}}} = \left(\frac{G^{p,d}_S S^{(p)}_A + G^{n,d}_S S^{(n)}_A}{G^{p,u}_S S^{(p)}_A + G^{n,u}_S S^{(n)}_A}\right)^2. \tag{46}$$

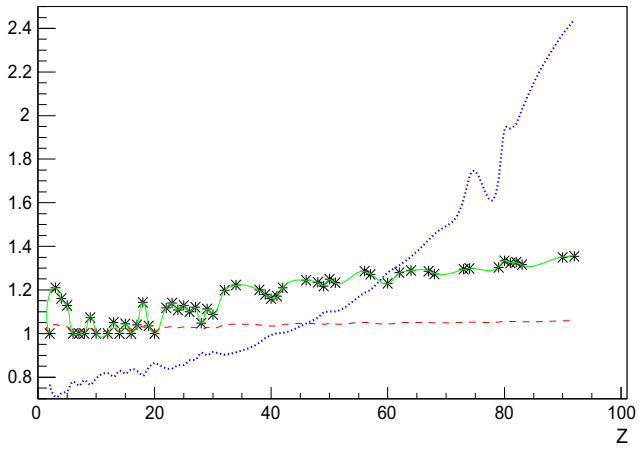

Fig. 2 This plot illustrates the prospects for distinguishing SI operators involving up quarks, from those involving down quarks, and vector operators from scalars. The continuous green [dashed red] line is the ratio, given in Eq. (45) [Eq. (46)], of $\mu \to e$ conversion rates induced by $\mathcal{O}^{uu}_{V,X}$ and $\mathcal{O}^{dd}_{V,X}$ [$\mathcal{O}^{uu}_{S,X}$ and $\mathcal{O}^{dd}_{S,X}$], assuming equal coefficients. The stars on the green line are an analytic approximation. The dotted blue line is the ratio, given in Eq. (47), of $\mu \to e$ conversion rates induced by $\mathcal{O}^{uu}_{V,X}$ and $\mathcal{O}^{uu}_{S,X}$, with coefficients selected to give the same rate on niobium ($Z = 41$)

For the $G_S^{N,q}$ values given in Appendix A, the scalar ratio is close to 1 (because $G_S^{p,q} \simeq G_S^{n,q}$), suggesting that changing the target in $\mu \to e$ conversion does not help distinguish $\mathcal{O}^{uu}_{S,X}$ from $\mathcal{O}^{dd}_{S,X}$.

The first and second leptoquark scenarios, respectively, induce scalar and vector operators. As discussed in [14,15], these can be distinguished by comparing the conversion rates in light and heavy targets. This is illustrated in Fig. 2, by the blue dotted line, which gives the double ratio normalised to niobium,

$$\left.\frac{\frac{\Gamma(Nb\mu\to Nbe)}{\Gamma((A,Z)\mu\to(A,Z)e)}}{\frac{\Gamma(Nb\mu\to Nbe)}{\Gamma((A,Z)\mu\to(A,Z)e)}}\right|_{\text{vector}}^{\text{scalar}} = \left(\frac{G_S^{p,u}S_{Nb}^{(p)} + G_S^{n,u}S_{Nb}^{(n)}}{G_S^{p,u}S_A^{(p)} + G_S^{n,u}S_A^{(n)}}\right)^2 \times \left(\frac{2V_A^{(p)} + V_A^{(n)}}{2V_{Nb}^{(p)} + V_{Nb}^{(n)}}\right)^2 . \quad (47)$$

We see that measuring the $\mu \to e$ conversion rate on aluminium, some intermediate target around $Z \sim 40$ and on a heavy nucleus like lead or gold (Z = 79), could distinguish the three leptoquark scenarios, that is, a vector operator involving ds vs. vector operator involving us vs. a scalar operator involving us.

5.2 Bounds on arbitrary coefficients of four operators

This section considers the operators induced by the second and third leptoquark models (see Eqs. (40) and (41)) which are added simultaneously to the Lagrangian with arbitrary coefficients:

$$\mathcal{L}_{EFT} = C^{uu}_{S,L}\mathcal{O}^{uu}_{S,L} + C^{uu}_{T,L}\mathcal{O}^{uu}_{T,L} + C^{dd}_{V,R}\mathcal{O}^{dd}_{V,R} + C^{dd}_{A,R}\mathcal{O}^{dd}_{A,R} + h.c. \quad (48)$$

This is clearly an incomplete basis (the complete basis of dimension six operators at μ_N is given in Eqs. (1) and (3)); however, it is sufficient for our purpose,[6] which is to explore which constraints can be obtained on quark-level operators from the non-observation of $\mu \to e$ conversion in targets with and without spin.

We suppose that $\mu \to e$ conversion has not been observed on aluminium, titanium (enriched in isotopes with spin) and lead targets. These targets are chosen because heavy and light targets have different sensitivities to vector and scalar coefficients, and because the spin of titanium and aluminium is, respectively, associated to an odd neutron and an odd proton. In order to check that upper bounds on these branching ratios can constrain all the operator coefficients which we consider, we set the branching ratios to 0, and we check that this forces the coefficients to vanish.

Setting the SD conversion rates in titanium and aluminium to zero gives two equations:

$$0 \simeq C^{dd}_{A,R}\left(G_A^{p,d} + \frac{S_n^{\text{Al}}}{S_p^{\text{Al}}}G_A^{n,d}\right) + 2C^{uu}_{T,L}\left(G_T^{p,u} + \frac{S_n^{\text{Al}}}{S_p^{\text{Al}}}G_T^{n,u}\right), \quad (49)$$

$$0 \simeq C^{dd}_{A,R}G_A^{n,d} + 2C^{uu}_{T,L}G_T^{n,u}, \quad (50)$$

where $\frac{S_n^{\text{Al}}}{S_p^{\text{Al}}} \simeq 0.1$ is the ratio of spin-expectation values in aluminium. These equations have solutions

$$2C^{dd}_{A,R} \simeq C^{uu}_{T,L}, \quad C^{dd}_{A,R} \simeq 2C^{uu}_{T,L},$$

so even allowing for a 10% theory uncertainty on the coefficients, it is clear that the only solution is for both coefficients to vanish. This is because the spin of titanium isotopes arises from the odd number of neutrons, whereas in aluminium the spin is from the odd proton, so these two conversion rates probe the SD coefficients $\widetilde{C}'^{NN}_{A,X}$ for both neutrons and protons. Then, since the matching coefficients $G^{Nu}_{A,X}$ and $G^{Nd}_{A,X}$ (equivalently $G^{Nu}_{T,X}$ and $G^{Nd}_{T,X}$) are of opposite sign and different magnitude, $C^{uu}_{A,X} + 2C^{uu}_{T,X}$ and $C^{dd}_{A,X} + 2C^{dd}_{T,X}$ can be distinguished.

It is straightforward to check that setting the SI rates on Al, Ti and Pb to zero, forces $C^{dd}_{V,R}, C^{uu}_{S,L} \to 0$.

A more informative way to present the constraints on coefficients arising from the experimental bounds is to give the covariance matrix. We suppose an upper bound of BR (for instance, 10^{-14}) on the SI branching ratios on Pb and Al, and

[6] In a later publication, we may try to constrain operator coefficients and count "flat directions", for which a complete basis would be required.

on the SD branching ratios on Al and Ti. The tensor operator gives comparable contributions to both SI and SD processes (see Appendix B), so the 4×4 covariance matrix does not split into 2×2 subblocks. Nonetheless, it is interesting to give the covariance matrices for different cases, in order to see the variation of the bounds, when different theoretical information is included.

First, the tensor contribution to the SI rates is neglected, in which case the covariance matrices for $(C^{dd}_{V,R}, C^{uu}_{S,L})$ and $(C^{uu}_{T,L}, C^{dd}_{A,R})$ are

$$\mathrm{BR}\begin{bmatrix} 0.012 & -0.0028 \\ -0.0028 & 0.0007 \end{bmatrix}, \quad \mathrm{BR}\begin{bmatrix} 9.1 & 20 \\ 20 & 73.6 \end{bmatrix}. \tag{51}$$

So, for instance, $|C^{uu}_{S,L}|$ is excluded above $\sqrt{0.0007 \times \mathrm{BR}}$, and $|C^{dd}_{A,R}| < \sqrt{73.6 \times \mathrm{BR}}$.

If now the SD rates are neglected, but the tensor contribution to SI is included, then the covariance matrix for $(C^{dd}_{V,R}, C^{uu}_{S,L}, C^{uu}_{T,L})$ is

$$\mathrm{BR}\begin{bmatrix} 0.47 & -0.24 & 23 \\ -0.24 & 0.13 & -14 \\ 23 & -14 & 1400 \end{bmatrix}, \tag{52}$$

which shows that the exclusions become weaker due to potential cancellations between a large $C^{uu}_{T,L}$ and the vector or scalar coefficients. Finally, the full covariance matrix arising from imposing $\mathrm{BR}_{\mathrm{SI}}(\mu\mathrm{Pb} \to e\mathrm{Pb}) \leq 10^{-14}$, $\mathrm{BR}_{\mathrm{SI}}(\mu\mathrm{Ti} \to e\mathrm{Ti}) \leq 10^{-14}$, $\mathrm{BR}_{\mathrm{SD}}(\mu\,{}^{47}\mathrm{Ti} \to e\,{}^{47}\mathrm{Ti}) \leq 10^{-14}$, $\mathrm{BR}_{\mathrm{SI}}(\mu\mathrm{Al} \to e\mathrm{Al}) \leq 10^{-14}$, and $\mathrm{BR}_{\mathrm{SD}}(\mu\mathrm{Al} \to e\mathrm{Al}) \leq 10^{-14}$, for the coefficients $(C^{dd}_{V,R}, C^{uu}_{S,L}, C^{uu}_{T,L}, C^{dd}_{A,R})$, is

$$\mathrm{BR}\begin{bmatrix} 0.010 & -0.0029 & 0.12 & 0.26 \\ -0.0029 & 0.0011 & -0.078 & -0.17 \\ 0.12 & -0.078 & 9.0 & 19.6 \\ 0.26 & -0.17 & 19.6 & 73 \end{bmatrix}. \tag{53}$$

Comparing with the bounds of Eq. (51), we see that the tensor contribution to the SI rate is of little importance, provided the SD bounds are included. However, if the SD bounds are neglected, including the tensor in the SI rate significantly weakens the constraints, as can be seen in Eq. (52). We also checked that including $\mathrm{BR}_{\mathrm{SI}}(\mu\mathrm{Au} \to e\mathrm{Au}) \leq 10^{-14}$ only changes a few entries by about 25%, as expected, because Al, Ti and Pb were chosen as targets for their discriminating power.

5.3 Reconstructing nucleon coefficients

We now suppose that $\mu \to e$ conversion is observed in aluminium, where there can be SI and SD contributions to the rate, and that the new physics is described by the nucleon-level Lagrangian of Eq. (5) with arbitrary operator coefficients. It is interesting to consider which subsequent targets, in what order, would be required to distinguish the SD and SI contributions, and then to discriminate among the SI operators?

We first introduce a geometric representation of models and targets, which allows one to visualise the ability of various targets to discriminate among models. A new physics scenario can be represented as a two 5-dimensional vectors, each composed of SI coefficients which interfere $\vec{C}_X \equiv (C_{D,X}, \widetilde{C}^{pp}_{S,X}, \widetilde{C}^{pp}_{V,Y}, \widetilde{C}^{nn}_{S,X}, \widetilde{C}^{nn}_{V,Y})$, and two two-component vectors of SD coefficients $(\widetilde{C}'^{nn}_{A,X}, \widetilde{C}'^{pp}_{A,X})$. For simplicity, we focus on $X = L$, and we drop this electron chirality subscript. Then we focus on discriminating among SI operators, because the spin of target nuclei is usually associated to either an unpaired n or p, giving an order of magnitude better sensitivity to the coefficient corresponding to the unpaired nucleon (see, e.g. the spin-expectation values given after Eq. (22)). This means that discriminating $\widetilde{C}'^{nn}_{A,X}$ vs. $\widetilde{C}'^{pp}_{A,X}$ should be a straightforward matter of using targets with an unpaired p and n.

For the spin-independent process, a target nucleus (Z, A) can be envisaged as a vector

$$\vec{v}_{(Z,A)} = (D_{(Z,A)}, S^{(p)}_{(Z,A)}, V^{(p)}_{(Z,A)}, S^{(n)}_{(Z,A)}, V^{(p)}_{(Z,A)}) \tag{54}$$

in the 5-dimensional coefficient space, whose components are the appropriate overlap integrals. (In the following, the vectors and components are indiscriminately labelled by A or Z because we use the overlap integrals of KKO, obtained for a single abundant isotope.) The matrix element for $\mu \to e$ conversion on target A, mediated by a combination of coefficients $\vec{C}$, is proportional to $\vec{C} \cdot \vec{v}_A$, and target nucleus A allows one to probe coefficients in the direction $\vec{v}_A$. If we define the unit-normalised $\hat{e}_A = \vec{v}_A/|\vec{v}_A|$, then target A probes the same combination of coefficients as aluminium if $\hat{e}_A$ is parallel to $\hat{e}_{\mathrm{Al}}$, and the difference

$$1 - \hat{e}_A \cdot \hat{e}_{\mathrm{Al}} \approx \frac{\theta^2}{2} \tag{55}$$

gives an invariant measure of whether the target A has sensitivity to an orthogonal direction in coefficient space. In Eq. (55), θ is the angle between $\hat{e}_A$ and $\hat{e}_{\mathrm{Al}}$. Figure 3 gives $\hat{e}_A \cdot \hat{e}_{\mathrm{Al}}$ as a function of Z. From Eq. (38), the uncertainty in the direction of $\hat{e}_A$ is $\lesssim 10\%$, so target A is indistinguishable from aluminium for $\hat{e}_A \cdot \hat{e}_{\mathrm{Al}} \gtrsim 0.995$, or $Z \lesssim 25$–30.

Perhaps a more transparent measure of the change of direction of $\hat{e}_A$ in coefficient space, is given in Fig. 4 by the ratio

$$e^O_A / e^O_{\mathrm{Al}} \tag{56}$$

where $O = \widetilde{C}^{pp}_{S,X}$ (continuous black), $O = \widetilde{C}^{nn}_{S,X}$ (dotted green), $\widetilde{C}^{pp}_{V,X}$ (dashed red) and $O = \widetilde{C}^{nn}_{V,X}$ (dot-dashed blue). Recall that e^O_A parametrises the fraction of the sensitivity of target A to operator O. So Fig. 4 shows that heavier targets have greater sensitivity to $\mathcal{O}^{nn}_V$ and less to $\mathcal{O}^{pp}_S$. (Unfortunately, this figure also suggests that $\mathcal{O}^{nn}_V$ and $\mathcal{O}^{pp}_S$ with

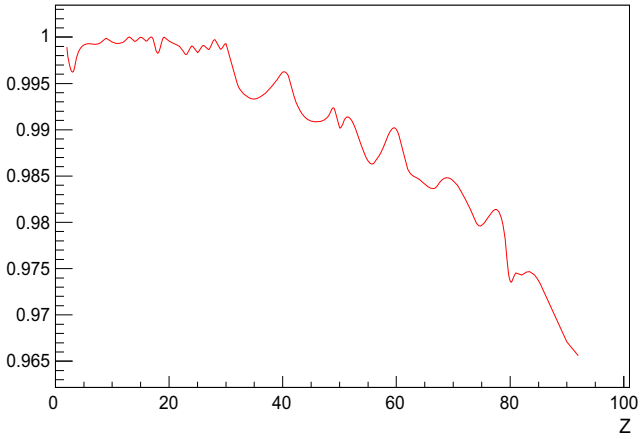

Fig. 3 A representation of the discriminating power of a target (labelled by Z), with respect to aluminium. On the vertical axis is the invariant measure, given in Eq. (55), of the misalignment in coefficient space of the target with respect to aluminium

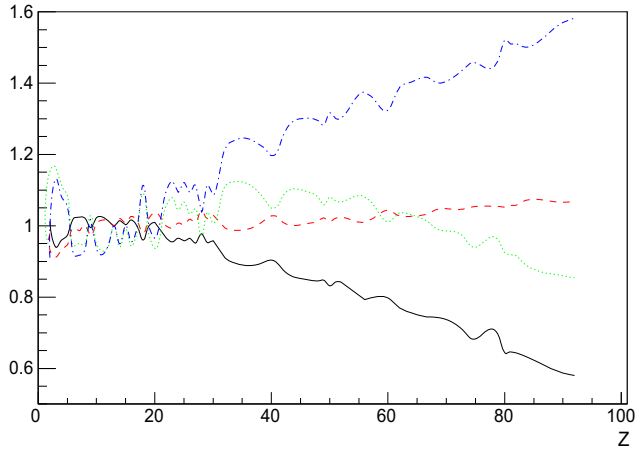

Fig. 4 An operator-dependent measure of the discriminating power of a targets (labelled by Z). On the vertical axis is the measure given in Eq. (56), of the relative sensitivity (normalised to aluminium) of a target to the operators $O = \widetilde{C}^{pp}_{S,X}$ (continuous black), $O = \widetilde{C}^{nn}_{S,X}$ (dotted green), $\widetilde{C}^{pp}_{V,X}$ (dashed red) and $O = \widetilde{C}^{nn}_{V,X}$ (dot-dashed blue)

comparable coefficients could be difficult to distinguish from $\mathcal{O}^{pp}_V$.) This normalised ratio of overlap integrals is interesting, because the normalisation "factors out" the growth with Z shared by all the overlap integrals, so this ratio parametrises the difference in direction in coefficient space, which allows different targets to discriminate among coefficients. This ratio also indicates that targets of $Z \lesssim 25$ cannot distinguish operators, if one admits a theory uncertainty of $\sim$10% in the calculation of the components e^O_A.

Assisted by the measures of discriminating power given in Eqs. (55) and (56), we now speculate on a possible series of targets. A light nucleus without spin could be an interesting second target, because it would allow one to distinguish whether the rate in aluminium was dominantly SD or SI. In particular, the SI rate in aluminium could be approximately predicted from the rate observed in another spinless light nucleus. This is because the SI rate in all targets with $Z \lesssim 20$ is sensitive to a similar linear combination of operator coefficients, as illustrated in Figs. 3 and 4.

An interesting choice for the second target could be titanium ($Z = 22$, $A = 48$). As illustrated in Figs. 3 and 4, it of sufficiently low Z that the SI rate probes the same combination of operator coefficients as the SI rate in aluminium. So measuring the SI rate in titanium-48 would allow one to determine whether there was a significant SD contribution to the $\mu \to e$ conversion rate observed on aluminium.

If there is indication for an SD contribution in aluminium, then it could be interesting to measure the rate on a titanium target enriched with the spin-carrying isotopes 47 and 49. This would give complementary information on the quark flavour of the tensor and/or axial vector operators, because the spin of aluminium is largely due to the odd proton, whereas for titanium there is an odd neutron. So the SD rate in aluminium is mostly sensitive to $\widetilde{C}'^{pp}_{A,X}$, whereas the SD rate in titanium depends on $\widetilde{C}'^{nn}_{A,X}$.

Finally, if there is no evidence of an SD rate in aluminium, a heavy target such as lead could be interesting to discriminate the scalar vs. vector coefficients in the SI rate.

6 Summary

This paper gives some details of the calculation of the spin-dependent (SD) $\mu \to e$ conversion rate in light nuclei, previously outlined in [18]. Section 2 reviews the operators involving quarks and gluons that contribute [14,15] at the experimental scale ($\mu_N = 2$ GeV), and matches them onto the nucleon operators which enter the nuclear physics calculation. Some attempt is made to include pion exchange in this matching (it is relevant because the momentum-transfer is m_μ^2). Section 3 calculates as much as possible of the conversion rate in the notation of relativistic, second-quantised, QFT [34]; in the last steps, the results of nuclear calculations are included. The final rate is given in Eq. (26). This section is not original; its purpose is to make the result accessible in the terminology of QFT. We recall the SD $\mu \to e$ conversion is incoherent, like SD WIMP scattering, so it is best searched for in light nuclei, where the $1/A^2$ suppression with respect to the coherent spin-independent (SI) rate (given in Eqs. (25) and (33)) is less significant.

Our SD rate estimate relies on nuclear physics calculations of the expectation value of nucleon axial currents in the nucleus. The results we use were obtained for SD WIMP scattering, which are often at zero momentum transfer. As discussed in point 6 of Sect. 3.1, additional nuclear calculations seem required to include tensor and pseudoscalar oper-

ators at finite momentum transfer, in light targets such as aluminium and titanium. In this paper, we did not discuss SD conversion on heavy nuclei; however, one can speculate that the nuclear expectation values could be of interest, because heavy nuclei could be sensitive to a different combination of tensor and axial operators from light nuclei. This is because the anti-lepton wavefunction contributes with opposite sign to the tensor vs. axial operators, and is more relevant in heavy nuclei (this sign difference allows one to discriminate scalar and vector operators in SI conversion on light and heavy nuclei [14]). Of course, the SD rate might be unobservably small (due to the $1/A^2$ suppression), but heavy nuclei could nonetheless give an independent constraint on the many operator coefficients.

Both the SD and the SI conversion rates depend on the modulus-squared of a sum of coefficients, weighted by nucleus-dependent numbers—see Eqs. (25), (26), and (33). This allows for cancellations, making it difficult to constrain individual coefficients, or identify the operators responsible for $\mu \to e$ conversion when it is observed. In the SI case, Kitano Koike and Okada (KKO) [14] pointed out that scalar vs. dipole vs. vector operators could be distinguished by changing the nuclear target. Section 5 explores, from various approaches, the prospects of distinguishing a wider variety of operators, including SD vs. SI, and u- vs. d-quark operators.

The prospects for discriminating vector or scalar operators involving either u or d quarks are illustrated in Fig. 2: vector operators involving u or d quarks could be distinguished by comparing the $\mu \to e$ conversion rate in light ($Z \lesssim 20$) and intermediate ($Z \sim 40$) targets, but distinguishing scalar u versus d operators seems difficult. Curiously, the u vs. d distinction is more transparent in the SD rates, as discussed after Eq. (50). So if both SD and SI conversion are observed, possibly the quark flavour could be extracted from the SD rates.[7]

The SD and SI contributions to the conversion rate could be distinguished (if the SD rate is large enough) by comparing the conversion rate in nuclei with and without spin. Section 4 reviews the theoretical uncertainties in the calculation of the $\mu \to e$ conversion rate, in order to estimate the sensitivity to the subdominant SD process. Comparing $\mu \to e$ conversion on isotopes with and without spin would cancel the leading theory uncertainties, giving a sensitivity (see the discussion after Eq. (37)) to $\Gamma_{\rm SD}/\Gamma_{\rm SI} \gtrsim \frac{0.1}{A}$, assuming a 10% uncertainty on $\Gamma_{\rm SI}$. Among the SD operators, it is not currently possible to distinguish pseudoscalar, axial and tensor coefficients, because only the nuclear expectation value of the axial operator has been calculated. However, as mentioned in the previous paragraph, it could be possible to discriminate SD operators involving u vs. d quarks, because they contribute differently in nuclei where the odd nucleon is a proton or neutron.

The upcoming COMET and Mu2e experiments will initially search for $\mu \to e$ conversion on aluminium, a target which has spin—so if they observe a signal, it could be mediated by the SD or SI operators. Therefore, in Sect. 5.3 we considered what series of subsequent targets could give information as regards the dominant coefficients. To this purpose, we represent a target material as a vector in the space of nucleon-level operators, whose components are numbers which multiply the operator coefficient in the rate (overlap integrals, in the SI case). Different targets can discriminate between operators, if they point in different directions of operator space. We plot in Figs. 3 and 4 two different measures of the misalignment between target vectors.

If $\mu \to e$ conversion is observed on aluminium, the following sequence of targets could be interesting: as second target, a light nucleus without spin, such as titanium-48, would discriminate whether the dominant contribution was from the SD rate, because the SI rate in titanium is comparable to aluminium (see Figs. 3, 4). If there is an SD contribution to the rate in aluminium, then titanium isotopes with spin, could be an interesting target: the spin of titanium is related to the odd neutron (whereas in aluminium there is an odd proton), so this could discriminate whether the SD operators involved u or d quarks. Finally, a heavy target such as gold or lead could allow one to discriminate scalar vs. vector operators, as pointed out in [14].

Acknowledgements We greatly thank Vincenzo Cirigliano for his participation in the early stages of this project, and for insightful discussions afterwards. SD acknowledges the partial support and hospitality of the Mainz Institute for Theoretical Physics (MITP) during the initial stages of this work. The work of YK is supported in part by the Japan Society of the Promotion of Science (JSPS) KAKENHI Grant no. 25000004.

A $G_O^{N,q}$

When the quark Lagrangian of Eq. (1) is matched onto the nucleon Lagrangian, the coefficients of the nucleon operators can be computed as $\widetilde{C}^{NN}_{O,Y} = \sum_q G_O^{N,q} C^{qq}_{O,Y}$, for $O \in T, A, V, P$; for the scalar operator there is an additional gluon contribution as described in [15]. We take the $G_O^{N,q}$, defined at zero momentum transfer such that $\langle N(P)|\bar{q}(x)\Gamma_O q(x)|N(P)\rangle = G_O^{N,q}\overline{u_N}(P)\Gamma_O u_N(P)$, to be

[7] Recall that SD and SI operators mix in the RG evolution, but without changing the quark flavour, as shown in Appendix C. The only flavour change is via the first two "penguin" diagrams of Fig. 5, which could change the flavour of vector operators.

$$G_V^{p,u} = G_V^{n,d} = 2, \quad G_V^{p,d} = G_V^{n,u} = 1, \quad G_V^{p,s} = G_V^{n,s} = 0, \tag{57}$$

$$G_A^{p,u} = G_A^{n,d} = 0.84(1), \quad G_A^{p,d} = G_A^{n,u} = -0.43(1),$$
$$G_A^{p,s} = G_A^{n,s} = -0.085(18), \tag{58}$$

$$G_S^{p,u} = \frac{m_p}{m_u} 0.021(2) = 9.0, \quad G_S^{p,d} = \frac{m_p}{m_d} 0.041(3) = 8.2,$$
$$G_S^{p,s} = \frac{m_N}{m_s} 0.043(11) = 0.42, \tag{59}$$

$$G_S^{n,u} = \frac{m_n}{m_u} 0.019(2) = 8.1, \quad G_S^{n,d} = \frac{m_n}{m_d} 0.045(3) = 9.0,$$
$$G_S^{n,s} \frac{m_N}{m_s} 0.043(11) = 0.42, \tag{60}$$

$$G_P^{p,u} = 144 = G_P^{n,d}, \quad G_P^{p,d} = -150 = G_P^{n,u},$$
$$G_P^{p,s} = -4.9 = G_P^{n,s}, \tag{61}$$

$$G_T^{p,u} = G_T^{n,d} = 0.77(7), \quad G_T^{p,d} = G_T^{n,u} = -0.23(3),$$
$$G_T^{p,s} = G_T^{n,s} = 0.008(9), \tag{62}$$

where the parentheses give the uncertainty in the last figure(s). The axial G_A are the results inferred in Ref. [52] by using the HERMES measurements [53]. The scalar G_S induced by light quarks are from a dispersive determination [54], and an average of lattice results [55] is used for the strange quark; in all cases, the $\overline{\text{MS}}$ quark masses at $\mu = 2$ GeV are taken as $m_u = 2.2$ MeV, $m_d = 4.7$ MeV, and $m_s = 96$ MeV [56]. The nucleon masses are $m_p = 938$ MeV and $m_n = 939.6$ MeV. The pseudoscalar results were calculated from data in the large-N_c approximation at $q^2 \approx 0$ [57], and here extrapolated to neutrons using isospin. The tensor results for the neutron are the lattice results of Cirigliano et al. [58], which are here extrapolated to protons using isospin.

For comparison, the G_A have been obtained on the lattice; a recent determination [59] is

$$G_A^{p,u} = G_A^{n,d} = 0.863(7)(14), \quad G_A^{p,d} = G_A^{n,u} = -0.345(6)(9),$$
$$G_A^{p,s} = G_A^{n,s} = -0.0240(21)(11). \tag{63}$$

The scalars $G_S^{N,q}$ have also recently been obtained on the lattice [60]:

$$G_S^{p,u} = \frac{m_p}{m_u} 0.0139(13)(12) = 5.9,$$
$$G_S^{p,d} = \frac{m_p}{m_d} 0.0253(28)(24) = 5.0, \tag{64}$$
$$G_S^{n,u} = \frac{m_n}{m_u} 0.0116(13)(11) = 5.0,$$
$$G_S^{n,d} = \frac{m_n}{m_d} 0.0302(3) = 6.0. \tag{65}$$

We observe that there is a 50% discrepancy with respect to the results of [54], obtained from pionic atoms and $\pi - N$ scattering [61]. Results similar to [54] were earlier obtained in [62], also using an effective theory.

B The tensor contribution to the SD and SI rates

We consider tensor operators,

$$C_{T,L}^{uu} \mathcal{O}_{T,L}^{uu} + C_{T,L}^{dd} \mathcal{O}_{T,L}^{dd} + \{L \leftrightarrow R\}, \tag{66}$$

at the experimental scale μ_N, which contribute at finite momentum transfer to the SI conversion process (see Eq. (19)), and also to the SD processes:

$$\frac{\Gamma_{\text{SI}}}{\Gamma_{\text{capt}}} = 8B_0 \frac{m_\mu^2}{m_N^2} |Z(C_{T,L}^{uu} G_T^{p,u} + C_{T,L}^{dd} G_T^{p,d}) F_p(m_\mu) + (A - Z)$$
$$\times (C_{T,L}^{uu} G_T^{n,u} + C_{T,L}^{dd} G_T^{n,d}) F_n(m_\mu)|^2 + \{L \leftrightarrow R\}, \tag{67}$$

$$\frac{\Gamma_{\text{SD}}}{\Gamma_{\text{capt}}} = 32B_0 \frac{J_A + 1}{J_A} \Big| S_p^A (C_{T,L}^{uu} G_T^{p,u} + C_{T,L}^{dd} G_T^{p,d})$$
$$+ S_n^A (C_{T,L}^{uu} G_T^{n,u} + C_{T,L}^{dd} G_T^{n,d}) \Big|^2 \frac{S_A(m_\mu)}{S_A(0)} + \{L \leftrightarrow R\}. \tag{68}$$

The ratio of these contributions, for a single operator, is

$$\frac{\Gamma_{\text{SD}}}{\Gamma_{\text{SI}}} \simeq 4 \frac{J_A + 1}{J_A} \frac{m_N^2}{m_\mu^2} \frac{\left| S_p^A G_T^{p,q} + S_n^A G_T^{n,q} \right|^2}{|Z G_T^{p,q} + (A - Z) G_T^{n,q}|^2}$$
$$\sim \begin{cases} 0.7 & q = u \quad A = \text{Al}, \\ 0.06 & q = d \quad A = \text{Al}, \\ 0.03 & q = u \quad A = \text{Ti}, \\ 0.01 & q = d \quad A = \text{Ti}, \end{cases} \tag{69}$$

where we assumed that the form factors are comparable $\frac{S_A(m_\mu)}{S_A(0)} \simeq |F_p(m_\mu)|^2$ as is the case in aluminium. Recall that $G_T^{n,u} \sim -\frac{1}{2} G_T^{p,u}$, so there is a partial cancellation in the SI amplitude, whereas the SD process arises mostly from an odd proton $S_p^A \gg S_n^A$, or mostly from an odd neutron $S_p^A \ll S_n^A$.

The estimates of Eq. (69) assume that only one tensor coefficient is non-zero, so they neglect interferences, which can easily enhance the SI rate. For instance, RG running of the tensor operator from the new physics scale to the experimental scale generically generates a scalar operator with comparable coefficient. The scalar–tensor interference contribution to the SI rate would be relatively enhanced, with respect to the tensor-squared, by $G_S^{N,q}/G_T^{N,q} \sim 10$, which would suppress the ratio in Eq. (69) by another factor 1/10.

C RG evolution

In this appendix, we review the renormalisation group evolution of operator coefficients from the leptoquark mass scale M ($\sim$ TeV) down to the experimental scale μ_N (2 GeV), via the one-loop RGEs of QCD and QED [19,20]. We consider the QED$\times$ QCD invariant operator basis discussed in Sect. 2. We neglect matching onto the SMEFT basis [63,64] and running with the full SM RGEs [65,66], on the assumption

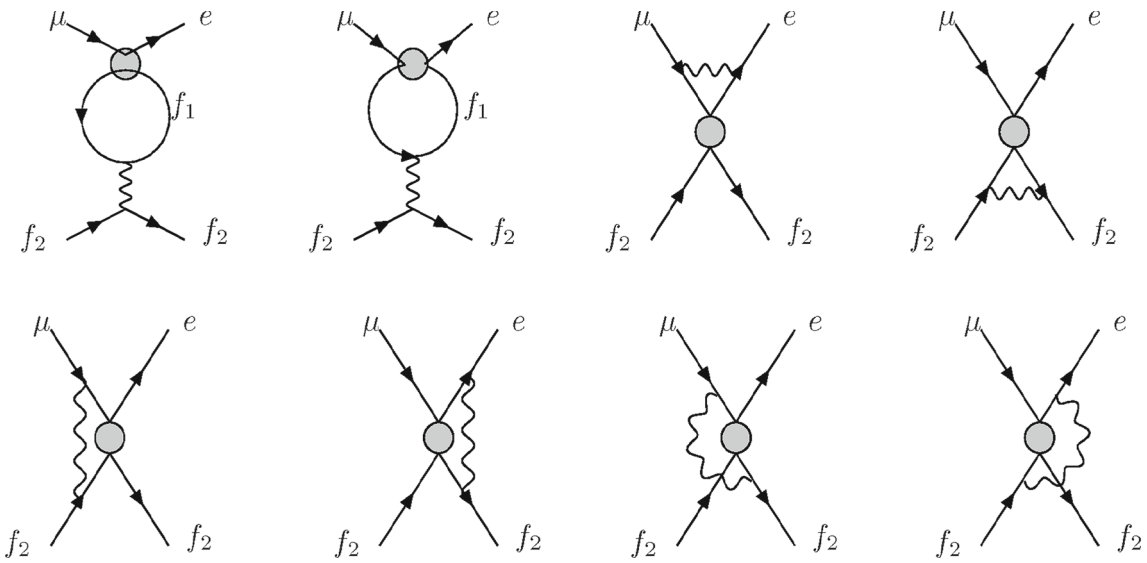

Fig. 5 Examples of one-loop gauge vertex corrections to four-fermion operators. The first two diagrams are the penguins. The last six diagrams contribute to operator mixing and running, but can only change the Lorentz or gauge structure of the operators, not the flavour structure. Missing are the wavefunction renormalisation diagrams; for $V \pm A$ Lorentz structure in the grey blob, this cancels diagrams 3 and 4

that QED is a reasonable approximation if M is not much larger than m_W.

After including one-loop corrections in the $\overline{\text{MS}}$ scheme, the operator coefficients will run with scale μ according to [19]

$$\mu \frac{\partial}{\partial \mu}(C_I, ...C_J, ...) = \frac{\alpha_e}{4\pi} \overrightarrow{C}\, \Gamma^e + \frac{\alpha_s}{4\pi} \overrightarrow{C}\, \Gamma^s \tag{70}$$

where I, J represent the super- and subscripts which label operator coefficients, Γ^e and Γ^s are the QED and QCD anomalous dimension matrices and $\overrightarrow{C}$ is a row vector that contains the QCD $\times$ QED invariant operators coefficients listed in Sect. 2.

In this work, we use the approximate analytic solution [18] given in Eq. (42):

$$C_I(\mu_N) = C_J(M)\lambda^{a_J}\left(\delta_{JI} - \frac{\alpha_e \widetilde{\Gamma}^e_{JI}}{4\pi} \log \frac{M}{\mu_N}\right)$$

where the factors are given after Eq. (42) and $\log \frac{M}{\mu_N} \sim 6.21$.

Only QED loops contribute to operators mixing, while QCD loops only rescale scalar and tensor operators. In Fig. 5, we present the QED diagrams required to compute the anomalous dimension γ of the four-fermion operators, where $f_1 \in \{e, \mu\}$ and $f_2 \in \{u, d, s, c, b, e, \mu, \tau\}$.

The operators coefficients below the scale M are organised in the vector $\overrightarrow{C}$ as follows:

$$\vec{C} = (\vec{C}^u_V, \vec{C}^d_V, \vec{C}^u_A, \vec{C}^d_A, \vec{C}^u_S, \vec{C}^d_S, \vec{C}^u_T, \vec{C}^d_T), \tag{71}$$

$$\vec{C}^f_V = (C^{ff}_{VL}, C^{ff}_{VR}) \quad \vec{C}^f_A = (C^{ff}_{AL}, C^{ff}_{AR}), \tag{72}$$

$$\vec{C}^f_S = (C^{ff}_{S,L}, C^{ff}_{S,R}) \quad \vec{C}^f_T = (C^{ff}_{T,L}, C^{ff}_{T,R}). \tag{73}$$

In the basis of $\overrightarrow{C}$, the QED anomalous dimension matrix can be written

$$\Gamma^e = \begin{bmatrix} \Gamma_{VA} & 0 \\ 0 & \Gamma_{\text{ST}} \end{bmatrix}$$

where

$$\Gamma_{\text{ST}} = \begin{bmatrix} \gamma^{u,u}_{S,S} & 0 & \gamma^{u,u}_{S,T} & 0 \\ 0 & \gamma^{d,d}_{S,S} & 0 & \gamma^{d,d}_{S,T} \\ \gamma^{u,u}_{T,S} & 0 & \gamma^{u,u}_{T,T} & 0 \\ 0 & \gamma^{d,d}_{T,S} & 0 & \gamma^{d,d}_{T,T} \end{bmatrix} \quad \text{and}$$

$$\Gamma_{VA} = \begin{bmatrix} 0 & 0 & \gamma^{u,u}_{V,A} & 0 \\ 0 & 0 & 0 & \gamma^{d,d}_{V,A} \\ \gamma^{u,u}_{A,V} & 0 & 0 & 0 \\ 0 & \gamma^{d,d}_{A,V} & 0 & 0 \end{bmatrix}. \tag{74}$$

Vector and axial operators

The first penguin diagram and the last four give the following matrices:

$$\gamma^{f,f}_{V,A} = \begin{array}{c|cc} & C^{ff}_{A,L} & C^{ff}_{A,R} \\ \hline C^{ff}_{V,L} & -12Q_f & 0 \\ C^{ff}_{V,R} & 0 & -12Q_f \end{array}, \quad \gamma^{f,f}_{A,V} = \begin{array}{c|cc} & C^{ff}_{V,L} & C^{ff}_{V,R} \\ \hline C^{ff}_{A,L} & 12Q_f & 0 \\ C^{ff}_{A,R} & 0 & 12Q_f \end{array}. \tag{75}$$

Using these anomalous dimension matrices and the RGEs gives

$$C^{qq}_{V,R}(\mu_N) = -3Q_q\frac{\alpha_e}{\pi}\log\frac{M}{\mu_N}C^{qq}_{A,L}(M) + C^{qq}_{V,R}(M), \tag{76}$$

$$C^{qq}_{A,R}(\mu_N) = 3Q_q\frac{\alpha_e}{\pi}\log\frac{M}{\mu_N}C^{qq}_{V,L}(M) + C^{qq}_{A,R}(M), \tag{77}$$

where $q \in \{u, d\}$. We see that axial operators mix to vector operators and vice versa, but there is no rescaling for axial and vector operators.

Scalar operators

Combining the third and fourth diagrams of Fig. 5 with the wavefunction diagrams renormalise the scalars while the last four diagrams mix the tensors to the scalars:

$$\gamma^{f,f}_{S,S} = \begin{array}{c|cc} & C^{ff}_{S,L} & C^{ff}_{S,R} \\ \hline C^{ff}_{S,L} & 6(1+Q_f^2) & 0 \\ C^{ff}_{S,R} & 0 & 6(1+Q_f^2) \end{array}, \quad \gamma^{f,f}_{T,S} = \begin{array}{c|cc} & C^{ff}_{S,L} & C^{ff}_{S,R} \\ \hline C^{ff}_{T,L} & -96Q_f & 0 \\ C^{ff}_{T,R} & 0 & -96Q_f \end{array}. \tag{78}$$

The scalars coefficients at the experimental scale read

$$C^{qq}_{S,L}(\mu_N) = 24\lambda^{a_T} f_{TS} Q_q \frac{\alpha_e}{\pi}\log\frac{M}{\mu_N}C^{qq}_{T,L}(M) + \lambda^{a_S}\left[1 - \frac{3}{2}\frac{\alpha_e}{\pi}\log\frac{M}{\mu_N}(1+Q_q^2)\right]C^{qq}_{S,L}(M). \tag{79}$$

Tensor operators

Similarly, the last four diagrams mix the scalars to the tensors. Only the wavefunction diagrams renormalise the tensors, because for the third and fourth diagrams $\gamma^\mu\sigma\gamma_\mu = 0$. We obtain the following matrices:

$$\gamma^{f,f}_{T,T} = \begin{array}{c|cc} & C^{ff}_{T,L} & C^{ff}_{T,R} \\ \hline C^{ff}_{T,L} & -2(1+Q_f^2) & 0 \\ C^{ff}_{T,R} & 0 & -2(1+Q_f^2) \end{array}, \quad \gamma^{f,f}_{S,T} = \begin{array}{c|cc} & C^{ff}_{T,L} & C^{ff}_{T,R} \\ \hline C^{ff}_{S,L} & 2Q_f & 0 \\ C^{ff}_{S,R} & 0 & 2Q_f \end{array}, \tag{80}$$

$$C^{qq}_{T,L}(\mu_N) = -\lambda^{a_S} f_{\mathrm{ST}} Q_q \frac{\alpha_e}{2\pi}\log\frac{M}{\mu_N}C^{qq}_{S,L}(M) + \lambda^{a_T}\left[1 + \frac{\alpha_e}{2\pi}\log\frac{M}{\mu_N}(1+Q_q^2)\right]C^{qq}_{T,L}(M). \tag{81}$$

Finally, the coefficients at the experimental scale μ_N are obtain via the matching condition,

$$\tilde{C}^{NN}_{O,Y}(\mu_N) = \sum_{q=u,d,s} G^{N,q}_O C^{qq}_{O,Y}(\mu_N). \tag{82}$$

References

1. A.M. Baldini et al. [MEG Collaboration], Search for the lepton flavour violating decay $\mu^+ \to e^+\gamma$ with the full dataset of the MEG experiment. Eur. Phys. J. C **76**(8), 434 (2016). https://doi.org/10.1140/epjc/s10052-016-4271-x. arXiv:1605.05081 [hep-ex]
2. U. Bellgardt et al. [SINDRUM Collaboration], Search for the decay $\mu \to 3e$. Nucl. Phys. B **299**, 1 (1988). https://doi.org/10.1016/0550-3213(88)90462-2
3. W.H. Bertl et al. [SINDRUM II Collaboration], A search for muon to electron conversion in muonic gold. Eur. Phys. J. C **47**, 337 (2006). https://doi.org/10.1140/epjc/s2006-02582-x
4. C. Dohmen et al. [SINDRUM II Collaboration], Test of lepton flavor conservation in $\mu \to e$ conversion on titanium. Phys. Lett. B **317**, 631 (1993)
5. W. Honecker et al. [SINDRUM II Collaboration], Improved limit on the branching ratio $\mu \to e$ conversion on lead. Phys. Rev. Lett. **76**, 200 (1996). https://doi.org/10.1103/PhysRevLett.76.200
6. K.A. Olive et al. [Particle Data Group], Chin. Phys. C**38**, 090001 (2014) and 2015 update
7. Y. Kuno [COMET Collaboration], A search for muon-to-electron conversion at J-PARC: The COMET experiment. PTEP **2013**, 022C01 (2013). https://doi.org/10.1093/ptep/pts089
8. R.M. Carey et al. [Mu2e Collaboration], Proposal to search for $\mu^- N \to e^- N$ with a single event sensitivity below 10^{-16}. FERMILAB-PROPOSAL-0973
9. Y. Kuno et al. (PRISM collaboration), An experimental search for a $\mu N \to eN$ conversion at sensitivity of the order of 10^{-18} with a highly intense muon source: PRISM. Unpublished, J-PARC LOI (2006)
10. S. Weinberg, G. Feinberg, Electromagnetic transitions between mu meson and electron. Phys. Rev. Lett. **3**, 111 (1959). https://doi.org/10.1103/PhysRevLett.3.111
11. O.U. Shanker, Z Dependence of coherent μe conversion rate in anomalous neutrinoless muon capture. Phys. Rev. D **20**, 1608 (1979). https://doi.org/10.1103/PhysRevD.20.1608
12. Y. Kuno, Y. Okada, Muon decay and physics beyond the standard model. Rev. Mod. Phys. **73**, 151 (2001). https://doi.org/10.1103/RevModPhys.73.151. arXiv:hep-ph/9909265
13. A. Czarnecki, W.J. Marciano, K. Melnikov, Coherent muon electron conversion in muonic atoms. AIP Conf. Proc. **435**, 409 (1998). https://doi.org/10.1063/1.56214. arXiv:hep-ph/9801218
14. R. Kitano, M. Koike, Y. Okada, Detailed calculation of lepton flavor violating muon electron conversion rate for various nuclei. Phys. Rev. D **66**, 096002 (2002). https://doi.org/10.1103/PhysRevD.76.059902. arXiv:hep-ph/0203110. (Erratum: [Phys. Rev. D **76** (2007) 059902])
15. V. Cirigliano, R. Kitano, Y. Okada, P. Tuzon, On the model discriminating power of $\mu \to e$ conversion in nuclei. Phys. Rev. D **80**, 013002 (2009). https://doi.org/10.1103/PhysRevD.80.013002. arXiv:0904.0957 [hep-ph]
16. H.C. Chiang, E. Oset, T.S. Kosmas, A. Faessler, J.D. Vergados, Coherent and incoherent (mu-, e-) conversion in nuclei. Nucl. Phys. A **559**, 526 (1993)
17. T.S. Kosmas, G.K. Leontaris, J.D. Vergados, Lepton flavor nonconservation. Prog. Part. Nucl. Phys. **33**, 397 (1994). https://doi.org/10.1016/0146-6410(94)90047-7. arXiv:hep-ph/9312217

18. V. Cirigliano, S. Davidson, Y. Kuno, Spin-dependent $\mu \to e$ conversion. Phys. Lett. B **771**, 242 (2017). https://doi.org/10.1016/j.physletb.2017.05.053. arXiv:1703.02057 [hep-ph]
19. S. Davidson, Mu to e gamma and matching at mW. arXiv:1601.07166 [hep-ph]
20. A. Crivellin, S. Davidson, G.M. Pruna, A. Signer, Renormalisation-group improved analysis of $\mu \to e$ processes in a systematic effective-field-theory approach. arXiv:1702.03020 [hep-ph]
21. U. Haisch, F. Kahlhoefer, On the importance of loop-induced spin-independent interactions for dark matter direct detection. JCAP **1304**, 050 (2013). https://doi.org/10.1088/1475-7516/2013/04/050. arXiv:1302.4454 [hep-ph]
22. A. Crivellin, F. D'Eramo, M. Procura, New constraints on dark matter effective theories from standard model loops. Phys. Rev. Lett. **112**, 191304 (2014). https://doi.org/10.1103/PhysRevLett.112.191304. arXiv:1402.1173 [hep-ph]
23. R. Machleidt, D.R. Entem, Chiral effective field theory and nuclear forces. Phys. Rep. **503**, 1 (2011). https://doi.org/10.1016/j.physrep.2011.02.001. arXiv:1105.2919 [nucl-th]
24. P. Klos, J. Menndez, D. Gazit, A. Schwenk, Large-scale nuclear structure calculations for spin-dependent WIMP scattering with chiral effective field theory currents. Phys. Rev. D **88**(8), 083516 (2013). https://doi.org/10.1103/PhysRevD.89.029901, https://doi.org/10.1103/PhysRevD.88.083516. arXiv:1304.7684 [nucl-th]. (Erratum: [Phys. Rev. D **89** (2014) no.2, 029901])
25. V. Cirigliano, M.L. Graesser, G. Ovanesyan, WIMP-nucleus scattering in chiral effective theory. JHEP **1210**, 025 (2012). https://doi.org/10.1007/JHEP10(2012)025. arXiv:1205.2695 [hep-ph]
26. M. Hoferichter, P. Klos, A. Schwenk, Chiral power counting of one- and two-body currents in direct detection of dark matter. Phys. Lett. B **746**, 410 (2015). https://doi.org/10.1016/j.physletb.2015.05.041. arXiv:1503.04811 [hep-ph]
27. A. Crivellin, M. Hoferichter, M. Procura, Accurate evaluation of hadronic uncertainties in spin-independent WIMP-nucleon scattering: disentangling two- and three-flavor effects. Phys. Rev. D **89**, 054021 (2014). https://doi.org/10.1103/PhysRevD.89.054021. arXiv:1312.4951 [hep-ph]
28. V. Cirigliano, W. Dekens, E. Mereghetti, A. Walker-Loud, Neutrinoless double beta decay in effective field theory: the light Majorana neutrino exchange mechanism. arXiv:1710.01729 [hep-ph]
29. A. Bartolotta, M.J. Ramsey-Musolf, Coherent $\mu - e$ conversion at next-to-leading order. arXiv:1710.02129 [hep-ph]
30. A. Pich, Effective field theory: course. arXiv:hep-ph/9806303
31. J. Engel, S. Pittel, P. Vogel, Nuclear physics of dark matter detection. Int. J. Mod. Phys. E **1**, 1 (1992). https://doi.org/10.1142/S0218301392000023
32. A.L. Fitzpatrick, W. Haxton, E. Katz, N. Lubbers, Y. Xu, The effective field theory of dark matter direct detection. JCAP **1302**, 004 (2013). https://doi.org/10.1088/1475-7516/2013/02/004. arXiv:1203.3542 [hep-ph]
33. J. Engel, M.T. Ressell, I.S. Towner, W.E. Ormand, Response of mica to weakly interacting massive particles. Phys. Rev. C **52**, 2216 (1995). https://doi.org/10.1103/PhysRevC.52.2216. arXiv:hep-ph/9504322
34. M.E. Peskin, D.V. Schroeder, *An Introduction to quantum field theory* (Addison-Wesley, Reading, 1995), p. 842
35. J.D. Bjorken, S.D. Drell, Relativistic quantum mechanics. "Relativistic quantum fields", ISBN-0070054940
36. M.E. Rose, *Relativistic Electron Theory* (Wiley, New York, 1961)
37. C. Itzykson, J.B. Zuber, *Quantum Field Theory* (Mcgraw-hill, New York, 1980). (International Series In Pure and Applied Physics)
38. H. De Vries, C.W. De Jager, C. De Vries, Nuclear charge and magnetization density distribution parameters from elastic electron scattering. At. Data Nucl. Data Tables **36**, 495 (1987). https://doi.org/10.1016/0092-640X(87)90013-1
39. M. Cirelli, E. Del Nobile, P. Panci, Tools for model-independent bounds in direct dark matter searches. JCAP **1310**, 019 (2013). https://doi.org/10.1088/1475-7516/2013/10/019. arXiv:1307.5955 [hep-ph]
40. T. Suzuki, D.F. Measday, J.P. Roalsvig, Total nuclear capture rates for negative muons. Phys. Rev. C **35**, 2212 (1987). https://doi.org/10.1103/PhysRevC.35.2212
41. V.A. Bednyakov, F. Simkovic, Nuclear spin structure in dark matter search: the zero momentum transfer limit. Phys. Part. Nucl. **36**, 131 (2005). arXiv:hep-ph/0406218. [Fiz. Elem. Chast. Atom. Yadra **36** (2005) 257]
42. V.A. Bednyakov, F. Simkovic, Nuclear spin structure in dark matter search: the finite momentum transfer limit. Phys. Part. Nucl. **37**, S106 (2006). https://doi.org/10.1134/S1063779606070057. arXiv:hep-ph/0608097
43. K.J.R. Rosman, P.D.P. Taylor, Pure Appl. Chem. **71**, 1593–1607 (1999)
44. J. Engel, P. Vogel, Phys. Rev. D **40**, 3132–3135 (1989)
45. G. Prezeau, A. Kurylov, M. Kamionkowski, P. Vogel, New contribution to wimp-nucleus scattering. Phys. Rev. Lett. **91**, 231301 (2003). https://doi.org/10.1103/PhysRevLett.91.231301. arXiv:astro-ph/0309115
46. C. Krber, A. Nogga, J. de Vries, First-principle calculations of dark matter scattering off light nuclei. Phys. Rev. C **96**(3), 035805 (2017). https://doi.org/10.1103/PhysRevC.96.035805. arXiv:1704.01150 [hep-ph]
47. F. Romeo [ATLAS and CMS Collaborations], Search for leptoquark-like signatures with the ATLAS and CMS detectors. Nucl. Part. Phys. Proc. **273–275**, 638 (2016). https://doi.org/10.1016/j.nuclphysbps.2015.09.096
48. V. Khachatryan et al. [CMS Collaboration], Search for pair production of first and second generation leptoquarks in proton–proton collisions at $\sqrt{s}$ = 8TeV. Phys. Rev. D **93**(3), 032004 (2016). https://doi.org/10.1103/PhysRevD.93.032004. arXiv:1509.03744 [hep-ex]
49. G. Aad et al. [ATLAS Collaboration], Searches for scalar leptoquarks in pp collisions at $\sqrt{s}$ = 8 TeV with the ATLAS detector. Eur. Phys. J. C **76**(1), 5 (2016). https://doi.org/10.1140/epjc/s10052-015-3823-9. arXiv:1508.04735 [hep-ex]
50. S. Bellucci, M. Lusignoli, L. Maiani, Nucl. Phys. B **189**, 329 (1981). https://doi.org/10.1016/0550-3213(81)90384-9
51. G. Buchalla, A.J. Buras, M.K. Harlander, Nucl. Phys. B **337**, 313 (1990). https://doi.org/10.1016/0550-3213(90)90275-I
52. G. Belanger, F. Boudjema, A. Pukhov, A. Semenov, Dark matter direct detection rate in a generic model with micrOMEGAs 2.2. Comput. Phys. Commun. **180**, 747 (2009). arXiv:0803.2360 [hep-ph]
53. A. Airapetian et al. [HERMES Collaboration], Precise determination of the spin structure function g(1) of the proton, deuteron and neutron. Phys. Rev. D **75**, 012007 (2007). https://doi.org/10.1103/PhysRevD.75.012007. arXiv:hep-ex/0609039
54. M. Hoferichter, J. Ruiz de Elvira, B. Kubis, U.G. Meiner, High-precision determination of the pion-nucleon term from Roy–Steiner equations. Phys. Rev. Lett. **115**, 092301 (2015). https://doi.org/10.1103/PhysRevLett.115.092301. arXiv:1506.04142 [hep-ph]
55. P. Junnarkar, A. Walker-Loud, Phys. Rev. D **87**, 114510 (2013). https://doi.org/10.1103/PhysRevD.87.114510. arXiv:1301.1114 [hep-lat]
56. K.A. Olive et al. [Particle Data Group], Chin. Phys. C **38**, 090001 (2014). https://doi.org/10.1088/1674-1137/38/9/090001
57. H.Y. Cheng, Low-energy interactions of scalar and pseudoscalar Higgs bosons with baryons. Phys. Lett. B **219**, 347 (1989). https://doi.org/10.1016/0370-2693(89)90402-4
58. T. Bhattacharya, V. Cirigliano, R. Gupta, H.W. Lin, B. Yoon, Neutron electric dipole moment and tensor charges from lattice QCD.

Phys. Rev. Lett. **115**(21), 212002 (2015). https://doi.org/10.1103/PhysRevLett.115.212002. arXiv:1506.04196 [hep-lat]
59. J. Green et al., Phys. Rev. D **95**(11), 114502 (2017). https://doi.org/10.1103/PhysRevD.95.114502. arXiv:1703.06703 [hep-lat]
60. S. Durr et al., Lattice computation of the nucleon scalar quark contents at the physical point. Phys. Rev. Lett. **116**(17), 172001 (2016). https://doi.org/10.1103/PhysRevLett.116.172001. arXiv:1510.08013 [hep-lat]
61. J. Ruiz de Elvira, M. Hoferichter, B. Kubis, U.G. Meiner, Extracting the sigma-term from low-energy pion-nucleon scattering. arXiv:1706.01465 [hep-ph]
62. J.M. Alarcon, J. Martin Camalich, J.A. Oller, The chiral representation of the πN scattering amplitude and the pion–nucleon sigma term. Phys. Rev. D **85**, 051503 (2012). https://doi.org/10.1103/PhysRevD.85.051503. arXiv:1110.3797 [hep-ph]
63. W. Buchmuller, D. Wyler, Effective Lagrangian analysis of new interactions and flavor conservation. Nucl. Phys. B **268**, 621 (1986). https://doi.org/10.1016/0550-3213(86)90262-2
64. B. Grzadkowski, M. Iskrzynski, M. Misiak, J. Rosiek, Dimension-six terms in the Standard Model Lagrangian. JHEP **1010**, 085 (2010). arXiv:1008.4884 [hep-ph]
65. R. Alonso, E.E. Jenkins, A.V. Manohar, M. Trott, Renormalization group evolution of the standard model dimension six operators III: Gauge coupling dependence and phenomenology. JHEP **1404**, 159 (2014). arXiv:1312.2014 [hep-ph]
66. E.E. Jenkins, A.V. Manohar, M. Trott, Renormalization group evolution of the standard model dimension six operators II: Yukawa dependence. JHEP **1401**, 035 (2014). https://doi.org/10.1007/JHEP01(2014)035. arXiv:1310.4838 [hep-ph]